Inorganic Chemistry

pubs.acs.org/IC

Article

N,N-Alkylation Clarifies the Role of *N*- and *O*-Protonated Intermediates in Cyclen-Based ^{64}Cu Radiopharmaceuticals

Alexander M. Brown, Jana L. Butman, Raphael Lengacher, Natasha P. Vargo, Kirsten E. Martin, Angus Koller, Dariusz Śmiłowicz, Eszter Boros,* and Jerome R. Robinson*

Cite This: *Inorg. Chem.* 2023, 62, 1362−1376

Read Online

ACCESS | Metrics & More | Article Recommendations | Supporting Information

ABSTRACT: Radioisotopes of Cu, such as ^{64}Cu and ^{67}Cu, are alluring targets for imaging (e.g., positron emission tomography, PET) and radiotherapeutic applications. Cyclen-based macrocyclic polyaminocarboxylates are one of the most frequently examined bifunctional chelators in vitro and in vivo, including the FDA-approved ^{64}Cu radiopharmaceutical, Cu(DOTATATE) (Detectnet); however, connections between the structure of plausible reactive intermediates and their stability under physiologically relevant conditions remain to be established. In this study, we share the synthesis of a cyclen-based, *N,N*-alkylated spirocyclic chelate, **H_2DO3A^{C4H8}**, which serves as a model for *N*-protonation. Our combined experimental (in vitro and in vivo) and computational studies unravel complex pH-dependent speciation and enable side-by-side comparison of *N*- and *O*-protonated species of relevant ^{64}Cu radiopharmaceuticals. Our studies suggest that *N*-protonated species are not inherently unstable species under physiological conditions and demonstrate the potential of *N,N*-alkylation as a tool for the rational design of future radiopharmaceuticals.

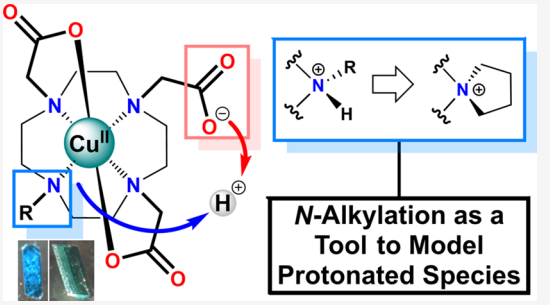

INTRODUCTION

Early recognition and treatment of cancer is imperative for patient survival,[1−3] which makes the advancement of theranostic tools and the unification of detection (e.g., positron emission tomography, PET) and therapy a decisive step toward improving life expectancy.[4−6] As access to cyclotron sources has become more readily available, radioisotopes of copper,[7−14] such as ^{64}Cu ($t_{1/2}$ = 12.7 h and β^+ = 653 keV) and ^{67}Cu ($t_{1/2}$ = 61.9 h and β^- = 141 keV), have received increasing attention as theranostic pairs.[13,15,16] Macrocyclic polyaminocarboxylates based on cyclen (i.e., **H_4DOTA** and **H_3DO3A**, Figure 1) have been examined extensively as bifunctional chelators[17−22] and comprise nearly half of all active ^{64}Cu clinical trials (Table S1).[23] [**^{64}Cu**]-**Cu**][**Cu^{II}(DOTATATE)**], Detectnet (Figure 1), was recently approved by the FDA and is currently the only ^{64}Cu agent indicated for use with PET for localization of somatostatin receptor positive neuroendocrine tumors in adults.[24−26] Successful tumor recognition requires that chelators maintain excellent stability in vivo, as delocalization of ^{64}Cu reduces imaging sensitivity (i.e., tumor recognition) and increases radiation exposure to off-target organs and tissues.[12] Although **H_4DOTA**, **H_3DO3A**, and their derivatives are well known to form thermodynamically and kinetically stable complexes in vitro, a number of studies have indicated challenges and diminished stability with the corresponding radiochemical Cu^{II} complexes.[27−31] Direct transchelation by biological ligands,[32,33] acid-mediated dissociation (hydrolysis),[34−36] and reduction-induced demetallation[37−39] have all been suggested as viable pathways for Cu^{II} decomplexation in vitro and/or in vivo; however, identification of key intermediates along these pathways has proven challenging.[40]

Over the past decades, several other classes of ^{64}Cu[Cu^{II}] chelators have been identified as suitable agents for PET.[4,12,13,41] Macrocyclic polyaminocarboxylates derived from cross-bridged (CB) cyclam provide impressive thermodynamic and kinetic stability through the constrained binding cavity;[37,42,43] however, these systems can require harsh and extended radiolabeling conditions incompatible with biological conjugating agents[44,45] without further modification.[46−48] Frameworks based on 1,4,7-triazacyclononane (tacn; e.g., NOTA) can display excellent stability and chelate ^{64}Cu[Cu^{II}] rapidly under mild conditions,[35,38,49,50] while further modifications to molecular charge, lipophilicity, and conjugation can lead to improved performance.[17,38,51−59] Pre-organized polycyclic *N*-donor chelates based on bispidine (bispa)[60−71] and sarcophagi (SarAr) scaffolds[72−85] can enable mild radiolabeling conditions and reasonable in vivo stability. Functionalization can be low yielding due to unselective

Received: August 12, 2022
Published: December 9, 2022

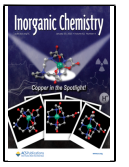

https://doi.org/10.1021/acs.inorgchem.2c02907
Inorg. Chem. 2023, 62, 1362−1376

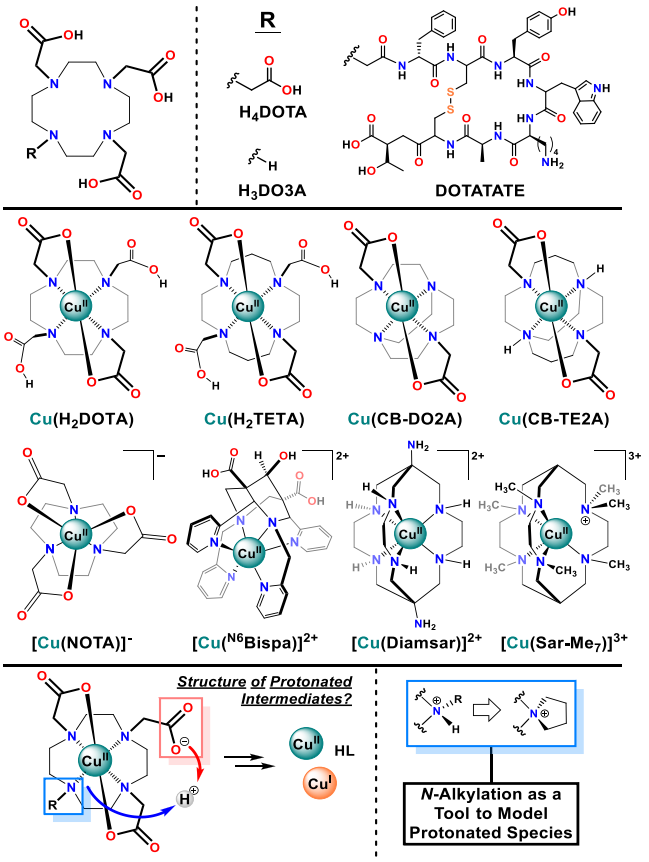

Figure 1. (*Top*) Cyclen-based polyaminocarboxylates and (*Mid*) select parent ^{64}Cu chelates. (*Bottom*) *N,N′*-Alkylation as a tool to model protonated species.

alkylation and the presence of multiple regioisomers; however, several effective approaches have been identified and clinical trials are ongoing.[72,80−82,86−89]

Given the variety of polyamino and polyaminocarboxylate chelators being screened as potential ^{64}Cu-based PET agents, the development of a working model for the structural speciation, reactivity, and plausible modes of decomplexation could guide the targeted development of future chelates. While single-crystal X-ray diffraction (SC-XRD) has provided valuable insight into the solid-state structures of the parent Cu^{II} cyclen-based polyaminocarboxylates (e.g., **$Cu^{II}(H_2DOTA)$** and **Cu^{II}(HDO3A)**),[90] much less is known regarding the structures of the relevant species in aqueous solution. Pereira observed several pH-dependent equilibria involving isomers of **$Cu^{II}(H_2DOTA)$** using electron paramagnetic resonance (EPR) spectroscopy, but the coordination geometries of these species were not assigned.[91] Aime followed the pH-dependent speciation for **Cu^{II}(HDO3A)** using electronic absorption spectroscopy, where a 35 nm blue shift in the d−d transition was observed moving from pH 3 to 2.[92] The blue shift was tentatively assigned to significant structural changes associated with protonation of the secondary amine and coordination of water moving from **Cu^{II}(HDO3A)** to **$[Cu^{II}(H_2DO3A)]^+$**.[93] Although there is a strong precedent for the protonation of macrocyclic amines to form out-of-cage intermediates involved in metal (de)complexation of *f*-elements,[94−107] the relevance of such species in the decomplexation of transition metals remains to be established.[35,37,92] Subsequent kinetic studies of acid-mediated hydrolysis of **Cu^{II}(HDO3A)** performed by Hermann suggested that *N*-protonation was kinetically inaccessible in the absence of excess acid; however, the identity of the relevant species remains unresolved.[35]

Identification of relevant protonated intermediates can be challenging as these species can display heightened reactivity and could be minor components of complex pH equilibria. Models of protonated species could deconvolute complex speciation and generate critical spectroscopic data to assign the identity of key species. Sargeson developed structural models for protonated quaternary ammonium sites in copper-bound SarAr ligands through N-methylation of these macrocyclic polyamines (Figure 1).[80] Although effective for these sarcophagine frameworks, the poor selectivity afforded by N-methylation of other polyamines has limited the effectiveness of such an approach. Alternatively, we envisioned selective double *N*-alkylation of a secondary amine to form a quaternary (4°) ammonium spirocycle that could serve as a model for *N*-protonated intermediates of Cu polyaminocarboxylates (Figure 1). Herein, we report the synthesis, characterization, and reactivity of a novel spirocyclic cyclen-based polyaminocarboxylate, **H_2DO3A^{C4H8}**, and its copper complex, **$Cu^{II}(DO3A^{C4H8})$**, to model possible *N*-protonated intermediates of **Cu^{II}(HDO3A)** and its derivatives. Through detailed spectroscopic and computational studies, we have determined that while *N*-protonation is predicted to be thermodynamically favorable for **Cu^{II}(HDO3A)**, both **Cu^{II}(HDO3A)** and **$Cu^{II}(H_2DO3A)^+$** exist as *O*-protonated isomers in solution. Despite their different structures, **$Cu^{II}(DO3A^{C4H8})$** and **Cu^{II}(HDO3A)** display comparable stability in vivo, which contrasts with expectations of Cu^{II} species supported by *N*-protonated macrocycles as inherently unstable and reactive intermediates along the dissociation pathway. These results highlight the importance of full structural characterization of inorganic radiopharmaceuticals and demonstrate the potential of *N*-alkylation as a tool for the rational design of future radiopharmaceuticals.

RESULTS AND DISCUSSION

Synthesis and Characterization of $[H_2DO3A^{C4H8}]$ and $[H^{OtBu}$DO3A]Br. Grams of analytically pure **$[H_2DO3A^{C4H8}]$** were obtained in 44% yield over two steps from **$[H^{OtBu}$DO3A]Br** without the need for chromatographic purification (Scheme 1). This was achieved through sequential alkylation of tert-butyl protected **$[H^{OtBu}$DO3A]Br** with 1,4-dibromobutane to yield **$[^{OtBu}DO3A^{C4H8}]$Br**, followed by

Scheme 1. Synthesis of $[H_2DO3A^{C4H8}]$: (i) $Br(CH_2)_4Br$ (1.5 equiv), K_2CO_3 (2 equiv), CH_3CN, 70 °C, 24 h, 72% Yield and (ii) CF_3COOH (20 equiv), CH_2Cl_2, RT, 12 h, 45% Yield

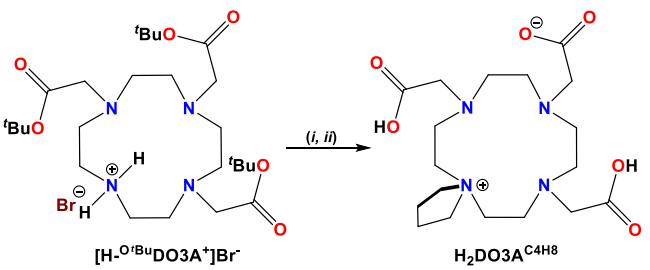

https://doi.org/10.1021/acs.inorgchem.2c02907
Inorg. Chem. 2023, 62, 1362−1376

deprotection with trifluoroacetic acid (TFA) to yield [H_2DO3A^{C4H8}].

SC-XRD experiments performed on [H^{OtBu}DO3A^{C4H8}][Br]$_2$ and [H_3DO3A^{C4H8}][Cl] unambiguously established macrocycle conformational preferences upon introduction of the spirocycle. [H^{OtBu}DO3A]Br and [H_5DO3A][SO_4] adopt the (2,3,3,4)-B macrocycle conformation (Figure 2),[108,109] while [H^{OtBu}DO3A^{C4H8}][Br]$_2$ and [H_3DO3A^{C4H8}][Cl] adopt the closely related (2,3,3,4)-A macrocycle conformation (Figures 2, S20, and S21). Moving from (2,3,3,4)-B to (2,3,3,4)-A placed the spirocycle in the least-hindered macrocycle position (i.e., corner), which minimized steric interactions between adjacent hydrogen atoms. Despite the minor differences in macrocycle conformation in the solid state, the introduction of the spirocycle into the cyclen-based frameworks did not perturb the global effective symmetry of [H^{OtBu}DO3A]Br and H_3DO3A in solution. Similar to [H^{OtBu}DO3A]Br and H_3DO3A, ^{1}H and ^{13}C NMR spectra of the isolated species, [^{OtBu}DO3A^{C4H8}]Br and H_2DO3A^{C4H8}, displayed effective C_s symmetry in solution (i.e., mirror plane bisecting the quaternary ammonium and *trans* nitrogen) and were consistent with facile macrocycle isomerization at room temperature (RT).

Aqueous potentiometric titrations revealed similarities between the acid−base behavior of H_2DO3A^{C4H8} and H_3DO3A (Table 1). H_2DO3A^{C4H8} displayed four pK_a values, one attributable to protonation of the tertiary amine *trans* to the spirocycle (pK_{a1}: 10.32) and three others below pH 5, which could include protonation of carboxylate and tertiary amine groups (pK_{a2-4}: 4.64, 3.55, and 1.42). Notably, pK_{a1-4} for H_2DO3A^{C4H8} are similar to pK_{a2-5} for H_3DO3A (ref 90: 100 mM KCl; pK_a: 11.59, 9.24, 4.43, and 3.48; this work: 100 mM $NaNO_3$; pK_a: 11.99, 9.61, 4.30, 3.63, and 1.84),[92]

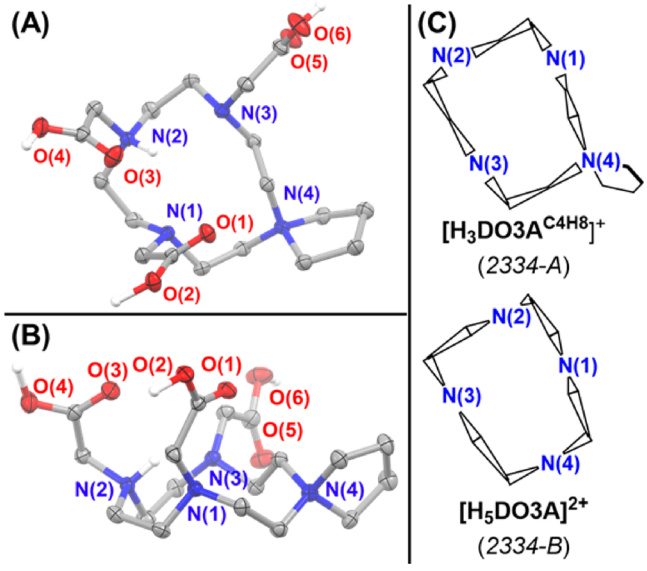

Figure 2. (A) Top and (B) side view of [H_3DO3A^{C4H8}][Cl] with thermal ellipsoids displayed at 50% probability. Counterions and H-atoms, except ammonium or carboxylic acid groups, were omitted for clarity. H-atoms attached to O(4) and O(6) are 50% occupied (located on Wyckhoff positions) and are homoconjugated with O(4)' and O(6)'. (C) Diagrams showing the stereochemistry and conformations of [H_3DO3A^{C4H8}]$^+$ and [H_5DO3A]$^{2+}$ in the solid state.

Table 1. Summary of pK_a Values for H_4DOTA,[a] H_3DO3A,[b] and H_2DO3A^{C4H8}[c]

L	H_4DOTA[a]	H_3DO3A[b,c]	H_2DO3A^{C4H8}[c]
pK_{a1}	11.41	11.59[b] (11.99)[c]	10.32
pK_{a2}	9.83	9.24[b] (9.61)[c]	4.64
pK_{a3}	4.38	4.43[b] (4.30)[c]	3.55
pK_{a4}	4.63	3.48[b] (3.44)[c]	1.42
pK_{a5}	1.92	(1.16)[c]	
pK_{a6}	1.58		

[a]Ref 91 (25.0 ± 0.1 °C and 0.1 M [NMe_4][Cl]). [b]Ref 90 (25.0 ± 0.1 °C and 0.1 M KCl). [c]25 °C and 0.1 M $NaNO_3$.

suggesting that the *N*,*N*-dialkylated spirocycle, H_2DO3A^{C4H8}, might serve as a viable model for *N*-protonation of H_3DO3A.

Potentiometric titrations of H_2DO3A^{C4H8} in the presence of $Cu^{II}(NO_3)_2$ (1.25:1, [L]:[Cu^{II}]; Figure S17) established H_2DO3A^{C4H8} as a competent chelate for Cu^{II}. Cu^{II}(DO3A^{C4H8}) remains the dominant Cu^{II} species down to pH 2.0, while curve-fitting provided an estimated stability constant ($\log(\beta_{Cu(L)})$) of 16.7. Although $\log(\beta_{Cu(L)}$ for Cu^{II}(DO3A^{C4H8}) is ∼6 orders of magnitude lower than [Cu^{II}(DO3A)]$^-$ ($\log(\beta_{Cu(L)}) = 22.9$), it is more stable than the protonated species, Cu^{II}(HDO3A), by ∼2 orders of magnitude ($\log(\beta_{Cu(HL)}) = 14.5$).[90]

Synthesis and Characterization of Cu^{II}(DO3A^{C4H8}). Encouraged by these findings, we pursued the synthesis of Cu^{II}(DO3A^{C4H8}). Cu^{II}(DO3A^{C4H8}) formed quantitatively within seconds of mixing aqueous solutions of [H_2DO3A^{C4H8}] and $Cu^{II}(OAc)_2$ at RT. Layering this solution with acetone (∼2:1 v/v) furnished high yields of dark blue crystals suitable for SC-XRD studies (Figure 3). Instead of the distorted octahedral, N_4O_2 coordination environment observed for the closely related and isoelectronic *O*-protonated species, Cu^{II}(H_2DOTA), Cu^{II}(HDO3A), and Cu^{II}(Me_2DO2A),[90,110] Cu^{II}(DO3A^{C4H8}) displays a distorted octahedral N_3O_3 coordination environment in the solid state. The equatorial plane consists of two N-donors and two O-donors [N(1), N(2), O(1), and O(5)], while the apical donors

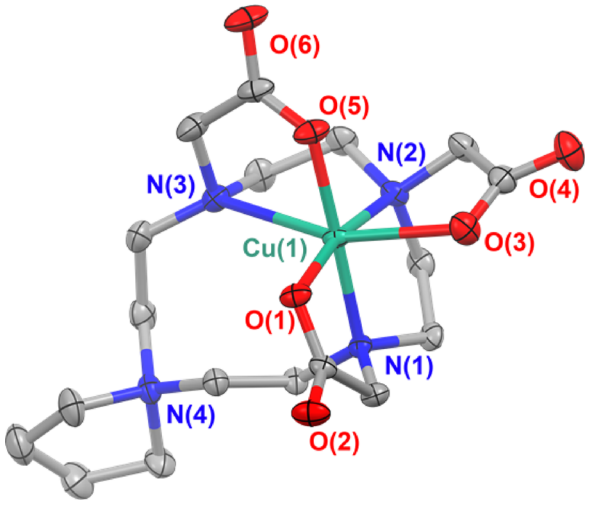

Figure 3. Thermal ellipsoid plot of Cu^{II}(DO3A^{C4H8}) displayed at 50% probability. Select bond metrics: Cu(1)−O(1), 1.975(13) Å, Cu(1)−O(3), 2.3160(14) Å, Cu(1)−O(5), 1.937(14) Å, Cu(1)−N(1), 2.010(15) Å, Cu(1)−N(2), 2.050(16) Å, Cu(1)−N(3), 2.611(1) Å, and Cu(1)−N(4), 4.444(1) Å.

https://doi.org/10.1021/acs.inorgchem.2c02907
Inorg. Chem. 2023, 62, 1362−1376

consist of N- and O-donors [N(3) and O(3)]. Distortion of the octahedral geometry is best reflected by the bond angle (∠O(3)−Cu(1)−N(3): 156.0° vs 180.0°) and the elongated apical distances (Cu(1)−O(3): 2.3160(13) Å, Cu(1)−N(3): 2.6111(15) Å). The observed deviations from an ideal octahedral environment arise both from the expected Jahn−Teller distortion,[111−113] as well as the distinct macrocyclic conformational constraint induced upon quaternization of N(4) compared to that of another N_3O_3 macrocycle, $[\mathbf{Cu^{II}(NOTA)}]^-$.[114−116] With our model complex in hand, we turned our attention to the solution structure of $\mathbf{Cu^{II}(DO3A^{C4H8})}$ and $\mathbf{Cu^{II}(HDO3A)}$ at variable pH.

Solution Spectroscopic Studies. Spectrophotometric titrations following the electronic absorption spectra of $\mathbf{Cu^{II}(HDO3A)}$ suggested that $[\mathbf{Cu^{II}(DO3A)}]^-$ should be the exclusive species formed at pH 7, while significant amounts of $\mathbf{Cu^{II}(HDO3A)}$ and $[\mathbf{Cu^{II}(H_2DO3A)}]^+$ formed below pH 5.[92] Although differences in λ_{max} and peak width were observed for $\mathbf{Cu^{II}(DO3A^{C4H8})}$ and $\mathbf{Cu^{II}(HDO3A)}$ (Figures S5 and S6), these solution measurements were insufficient to fully assign the structure of these species. Therefore, we performed variable pH X-band EPR measurements (pH = 7, 5, and 3) on degassed, frozen solutions of $\mathbf{Cu^{II}(DO3A^{C4H8})}$ and $\mathbf{Cu^{II}(HDO3A)}$ to establish the structure of protonated species in solution (Figure 4 and Table 2; [Cu^{II}] ∼10 mM, [$NaClO_4$] = 100 mM, 77 K).

$\mathbf{Cu^{II}(DO3A^{C4H8})}$ exists as single species over the pH range of 3−7 and displays an axial spectrum ($g_e < g_x \sim g_y < g_z$) that is consistent with the axially elongated, distorted octahedral geometry and N_3O_3 binding mode found in the solid state ($g_\perp$:$g_x = g_y$ = 2.056 G; $g_\parallel$:g_z = 2.272 G, $A_x = A_y = 19 \times 10^{-4}$ cm^{-1}; $A_z = 176 \times 10^{-4}$ cm^{-1}).[117−119] Both g_z and g_x, g_y compare favorably to axially elongated, distorted octahedral N_4O_2 species, $\mathbf{Cu^{II}(TEBIDA)(bpy)(OH_2)}$ (TEBIDA: *N*-tert-butyliminodiaceticacid; $g_\perp$:$g_x = g_y$ = 2.05 G; $g_\parallel$:g_z = 2.29 G; $Cu-N_{eq(avg)}$ = 2.013(5) Å, $Cu-O_{eq(avg)}$ = 1.962(5) Å, $Cu-N_{ax}$ = 2.483(6) Å, $Cu-O_{ax}$ = 2.512(5) Å; and $O_{ax}-Cu-N_{ax}$ = 153.2°).[120] This provides further support that the distorted octahedral geometry observed in the solid state is maintained in solution.

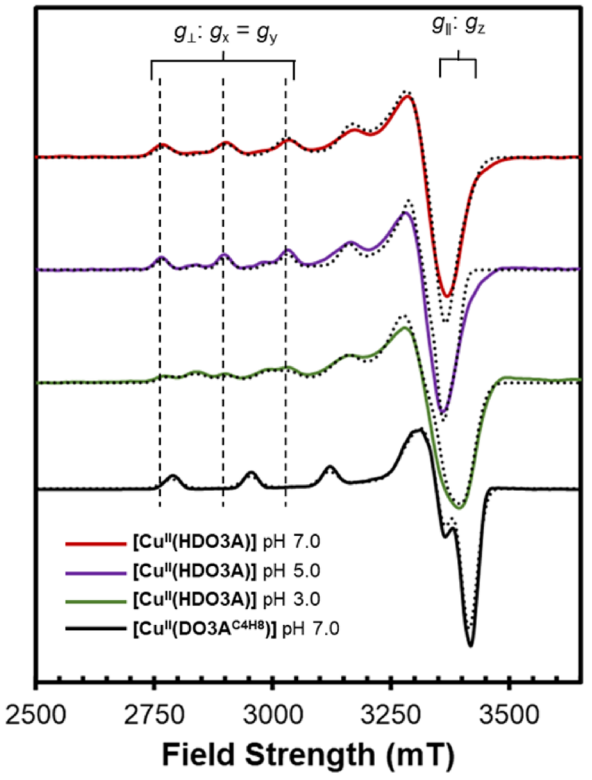

Figure 4. Variable pH X-band (9.65 GHz) EPR spectra of $\mathbf{Cu^{II}(HDO3A)}$ (pH = 7, 5, 3) and $\mathbf{Cu^{II}(DO3A^{C4H8})}$ (pH = 7) with $NaClO_4$ (100 mM).

Having established a clear signature for an *N*-protonated isomer, we turned our attention to the variable pH speciation of $\mathbf{Cu^{II}(HDO3A)}$ (Figure 4). At pH 7, $[\mathbf{Cu(DO3A)}]^-$ also exists as single species with an axial spectrum consistent with the tetragonal N_4O_2 binding mode observed for $\mathbf{Cu^{II}(HDO3A)}$ in the solid state ($g_\perp$:$g_x = g_y$ = 2.075 G; $g_\parallel$:g_z = 2.319 G; $A_x = A_y = 32 \times 10^{-4}$ cm^{-1}; and $A_z = 170 \times 10^{-4}$ cm^{-1}) and comparable to that of $[\mathbf{Cu^{II}(DOTA)}]^{2-}$ (77 K, pH = 7; g_z = 2.300 G; and $g_x = g_y$ = 2.070 G).[91,121,122] At pH 5, second species formed in a ∼3:1 ratio, which further increased in abundance at pH 3 (∼1:2 ratio). This second species also displayed an axial spectrum, but with *g* values ($g_\perp$:$g_x = g_y$ = 2.060 G; $g_\parallel$:g_z = 2.247 G; $A_x = A_y = 13 \times 10^{-4}$ cm^{-1}; and $A_z = 133 \times 10^{-4}$ cm^{-1}) distinct from the distorted octahedral N_3O_3 binding mode found in $\mathbf{Cu^{II}(DO3A^{C4H8})}$ and the distorted octahedral N_4O_2 of $[\mathbf{Cu^{II}(DO3A)}]^-$. Deviations from the ideal g_e (2.0023) arise from spin−orbit coupling contributions, which can be quenched to varying degrees depending on ligand-field effects. In the case of axial Cu^{II} spectra, a decrease in g_z implicates increased *equatorial* ligand field strength, which could be due to ligand substitution or decreased tetragonal distortion.[119,121−125] The decreased g_z and A_z values for $\mathbf{Cu^{II}(HDO3A)}$ at lower pH are consistent with increased axial elongation and/or transition to a square pyramidal geometry, which when considering the spectral differences between $\mathbf{Cu^{II}(HDO3A)}$ and $\mathbf{Cu^{II}(DO3A^{C4H8})}$, must be a consequence of *O*-protonation. A similar square-pyramidal geometry was proposed by Di Marco and coworkers for the mono-protonated species, $[\mathbf{Cu^{II}(HDO2A2S)}]^+$ (DO2A2S: 1,7-bis-[2-(methylsulfanyl)ethyl]-4,10-diacetic acid-1,4,7,10-tetraaza-cyclododecane), which was the lowest energy species predicted by density functional theory (DFT) calculations.[39]

Computational Studies. To provide further support for our structural assignments and better understand the speciation landscape of $\mathbf{Cu^{II}(H_xDO3A)}$ (x = 0, 1, 2), we performed DFT calculations in water using implicit solvation at the M06-L[126] level of theory (see the Supporting Information for further details). The local meta-GGA functional, M06-L, was selected due to its ability to accurately reproduce Cu^{II} geometries with relatively low computational cost,[126−130] while an ECP10MWB contracted pseudopotential basis set and 6−31(d′,p′) basis set were used for Cu^{II} and C, H, N, and O, respectively. Geometry-optimized structures of $\mathbf{Cu^{II}(DO3A^{C4H8})}$ and $\mathbf{Cu^{II}(HDO3A)}$ were obtained starting from the coordinates of the diffraction experiments, where the calculated structures were in good agreement with those obtained by the experiment. Only minor deviations were observed in the bond lengths and angles associated with the primary coordination sphere of the minimized structures (mean-unsigned error; MUE($\mathbf{Cu^{II}(DO3A^{C4H8})}$) = 0.036, MUE($\mathbf{Cu^{II}(HDO3A)}$) = 0.033), and confirmed the suitability of the selected level of theory for further speciation studies.

Geometry optimization of plausible isomers of $\mathbf{Cu^{II}(HDO3A)}$ led to the identification of four low-energy

https://doi.org/10.1021/acs.inorgchem.2c02907
Inorg. Chem. 2023, 62, 1362−1376

Table 2. Summary of EPR g Tensors and Hyperfine Coupling Constant Values for $Cu^{II}(HDO3A)$ and $Cu^{II}(DO3A^{C4H8})$

compound[a]	pH	g_x	g_y	g_z	$A_x(\times10^{-4}$ cm$^{-1})$	$A_y(\times10^{-4}$ cm$^{-1})$	$A_z(\times10^{-4}$ cm$^{-1})$	(%)
$Cu^{II}(HDO3A)$	7	2.075	2.075	2.317	32	32	170	100
$Cu^{II}(HDO3A)$	5	2.075	2.075	2.317	32	32	170	~75
$[Cu^{II}(H_2DO3A)]^+$	5	2.060	2.060	2.247	13	13	133	~25
$Cu^{II}(HDO3A)$	3	2.075	2.075	2.317	32	32	170	~40
$[Cu^{II}(H_2DO3A)]^+$	3	2.060	2.060	2.247	13	13	133	~60
$Cu^{II}(DO3A^{C4H8})$	3–7	2.056	2.056	2.273	19	19	176	100

[a]Obtained at 9.65 GHz at 77 K in a glass composed of 50:50 ethylene glycol/H_2O, 100 mM $NaClO_4$. g and A values obtained from fits using EasySpin.

species within a ~3 kcal/mol range (Figure 5). Although the *O*-protonated isomer identified by X-ray diffraction experiments, ***O*-N_4O_2-Cu^{II}(HDO3A)** (distorted octahedral), was a low energy structure, the corresponding *N*-protonated structure, ***N*-N_3O_3-Cu^{II}(HDO3A)** (square-pyramidal), was 1 kcal/mol more stable. Alternative *O*-protonated structures, ***O*-N_3O_2-Cu^{II}(HDO3A)** (square-pyramidal), ***O*-N_4O_1-Cu^{II}(HDO3A)** (square-pyramidal), and ***O*-N_2O_3-Cu^{II}(HDO3A)** (trigonal bipyramidal) were also found to be

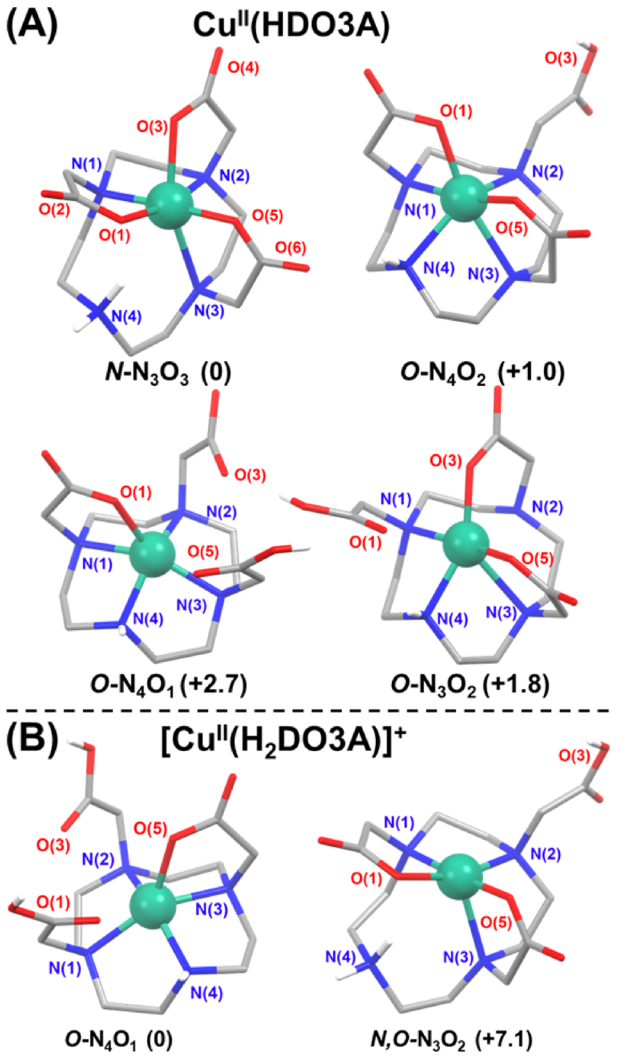

Figure 5. Capped-stick images of the lowest energy isomers (relative energies, kcal/mol) identified by DFT for (A) **Cu^{II}(HDO3A)** and (B) **$[Cu^{II}(H_2DO3A)]^+$**. H-atoms other than those residing on heteroatoms have been removed for clarity.

~1 to 2 kcal/mol higher in energy than ***O*-N_4O_2-Cu^{II}(HDO3A)**. While ***N*-N_3O_3-Cu^{II}(HDO3A)** was predicted to be lowest in energy by ~1 kcal/mol, the calculated structure closely matched that of **$Cu^{II}(DO3A^{C4H8})$** (MUE = 0.023), which would be expected to display effectively identical g and A values. The small energy differences between ***N*-N_3O_3-Cu^{II}(HDO3A)** and several other isomers (~1 kcal/mol) are well within the error of the calculation, especially when considering additional solvent stabilization effects, which might not be captured with implicit solvation techniques. Based on the results of our theoretical studies and literature EPR measurements on related compounds, the isomers most consistent with our EPR measurements and theory-predicted energetics would be ***O*-N_4O_2-Cu^{II}(HDO3A)** (distorted octahedral) and ***O*-N_4O_1-Cu^{II}(HDO3A)** (square-pyramidal).

The predicted speciation profile of **$[Cu^{II}(H_2DO3A)]^+$** was much more clear-cut. The doubly *O*-protonated isomer, ***O*-N_4O_1-$[Cu^{II}(H_2DO3A)]^+$** (square-pyramidal), was identified as the lowest energy structure, while the mixed *N*- and *O*-protonated isomer, ***N,O*-N_3O_2-$[Cu^{II}(H_2DO3A)]^+$**, the next lowest isomer, was 7.1 kcal/mol higher in energy. Notably, the square-pyramidal ***O*-N_4O_1-$[Cu^{II}(H_2DO3A)]^+$** structure would be consistent with the axial spectrum and range of g-values observed by EPR. While H_2O-bound species were previously hypothesized, especially in the context of *N*-protonation,[92] no geometry-optimized structures of **Cu^{II}(HDO3A)** and **$[Cu^{II}(H_2DO3A)]^+$** with water-coordinated could be identified in our study. Taken together, both EPR and DFT support that **Cu^{II}(HDO3A)** exists predominantly as ***O*-N_4O_2-Cu^{II}(HDO3A)**, the distorted octahedral species identified by X-ray crystallography. Upon decreasing pH, a second oxygen is protonated and the structure transitions to **N_4O_1-$[Cu^{II}(H_2DO3A)]^+$**, square pyramidal species whose structure has not been previously characterized.

Crystallization of $[Cu^{II}(H_2DO3A)][Br]$. Intrigued by the presence of an unaccounted-for isomer at low pH, crystallization of **$[Cu^{II}(H_2DO3A)]^+$** was pursued. Dark-blue, X-ray quality single crystals of **$[Cu^{II}(H_2DO3A)]Br$** were obtained in 34% yield from acetone layered aqueous solutions of **Cu^{II}(HDO3A)** and NH_4Br adjusted to pH 3 (Figure 6). **$[Cu^{II}(H_2DO3A)]Br$** featured a five-coordinate, distorted square-pyramidal Cu^{II} coordinated by **H_2DO3A** in an N_4O_1 binding mode. The single carboxylate [O(5)] occupied the apical position of the distorted square pyramid, while the cyclen N-donors made up the equatorial base [N(1)–N(4)]. Notably, protonation occurred at two adjacent carboxylate sites [O(1) and O(3)], both of which remain unbound [Cu–O(1) = 2.964(2) Å, Cu–O(3) = 3.170(2) Å] and engaged in hydrogen-bonding interactions with interstitial water molecules (Figure S23). This structure was distinct from that of *N,N′*-diprotonated out-of-cage species observed for *f*-block

https://doi.org/10.1021/acs.inorgchem.2c02907
Inorg. Chem. 2023, 62, 1362–1376

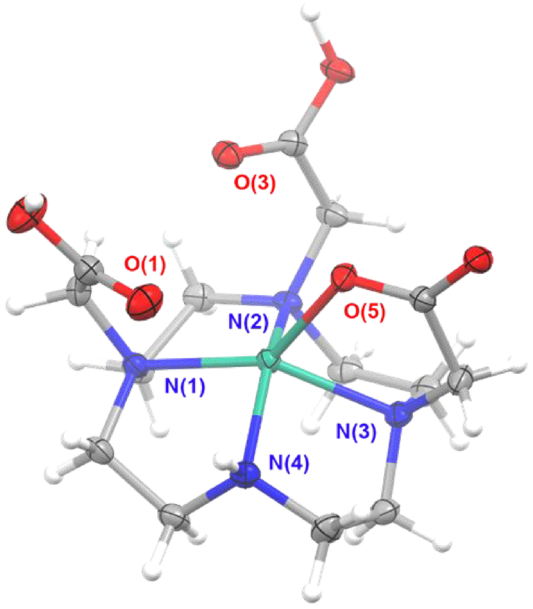

Figure 6. Thermal ellipsoid plot (50% probability) of [$\mathbf{Cu^{II}(H_2DO3A)}$]**Br**. Br^- and interstitial H_2O not displayed for clarity.

elements[94−107] or polymetallic Fe^{III} clusters.[131] Notably, Anderson and coworkers isolated and crystallographically characterized Cu^{II} species supported by *O*-monoprotonated and *O*,*O*′-diprotonated CB cyclam derivatives, yet, unlike [$\mathbf{Cu^{II}(H_2DO3A)}$]**Br**, the pendant carboxylic acid arm(s) remains coordinated.[132] The distorted square-pyramidal geometry and primary coordination sphere of [$\mathbf{Cu^{II}(H_2DO3A)}$]**Br** was consistent with the dominant species we observed by EPR at pH 3 and matches well with the DFT-calculated structure (vide infra and Figure S30, MUE = 0.067).

Kinetic Stability: Acid-Mediated Dissociation and Reduction-Induced Demetallation. While *N*- and *O*-protonated species have been invoked as key reactive intermediates involved in the chelation and decomplexation of Cu in aqueous media,[32,35,133] structure−function relationships linking in vitro and in vivo stability of these species remain to be established. Acid-mediated dissociation studies are routinely employed to estimate kinetic inertness,[34−36] although they are not a reliable predictor of in vivo stability.[134−136] The half-lives for acid-mediated dissociation ($t_{1/2}$) were determined from 3 mM solutions of $\mathbf{Cu^{II}(DO3A^{C4H8})}$ and $\mathbf{Cu^{II}(HDO3A)}$ exposed to 1 M HCl at RT using UV−vis spectroscopy (Figure S24). Decomplexation occurred ∼60-fold faster for $\mathbf{Cu^{II}(DO3A^{C4H8})}$ compared to $\mathbf{Cu^{II}(HDO3A)}$ ($t_{1/2}$ = 83.50 ± 1.40 vs 1.40 ± 0.02 min, respectively) and implicates lower kinetic stability of *N*- versus *O*-protonated Cu^{II} complexes at extremely low pH (∼0).

In the appropriate coordination environment, Cu^{II} can be reduced by typical bioreductants found in vivo (−0.4 V vs NHE), and the resulting Cu^{I} species may be more susceptible to transchelation and dissociation in vivo.[137] This has been termed reduction-induced demetallation,[37−39] and variable pH voltammetry has emerged as a useful technique to interrogate this pathway on the ms to s timescale.[37,38,132,138−141] In water, dissociation of free Cu^{I} will rapidly disproportionate and plate Cu^0 on the electrode surface, which will generate a characteristic stripping feature upon scanning to sufficiently oxidizing potentials ($Cu^{0/II}$, E_{pa} ∼ +0.1 V vs Ag/AgCl).[141−144] At pH 7, $\mathbf{Cu^{II}(DO3A^{C4H8})}$ and $\mathbf{Cu^{II}(HDO3A)}$ displayed quasi-reversible $Cu^{II/I}$ couples (Figure 7; $E_{1/2}$ = −0.62 and −0.74 V vs Ag/AgCl, respectively). Given the increasing appreciation for the effects of cations on modulating the redox potential of redox-active metals,[145−149] it may be tempting to attribute the 120 mV positive shift moving from $\mathbf{Cu^{II}(HDO3A)}$ to $\mathbf{Cu^{II}(DO3A^{C4H8})}$ to the introduction of a positive charge in the framework; however, this could also be readily attributed to the changes in geometry and donor number, since it is well-established that the $Cu^{II/I}$ redox couple is sensitive to donor identity, coordination number, and geometry.[150] Regardless, both chelates significantly stabilize the Cu^{II} oxidation-state and disfavor reduction-induced demetallation at pH 7 (Figures S7b and S8b). At pH 5, $\mathbf{Cu^{II}(DO3A^{C4H8})}$ displays signs of limited reduction-induced demetallation, whereas $\mathbf{Cu^{II}(HDO3A)}$ remains kinetically inert on the CV timescale. At pH 3, both complexes undergo reduction-induced demetallation; however, $\mathbf{Cu^{II}(HDO3A)}$ loses all reversibility and the $Cu^{0/II}$ stripping feature is ∼fivefold greater than that of $\mathbf{Cu^{II}(HDO3A^{C4H8})}$. Encouraged by the electrochemical stability at pH 7, we examined the behavior of the corresponding ^{64}Cu-labeled complexes under physiologically relevant conditions.

Radiolabeling and Biodistribution. $\mathbf{H_2DO3A^{C4H8}}$ and $\mathbf{H_3DO3A}$ readily complex [^{64}Cu][$CuCl_2$] (25−30 μCi; Figure S25) to form [$\mathbf{^{64}Cu}$][$\mathbf{Cu^{II}(DO3A^{C4H8})}$] and [$\mathbf{^{64}Cu}$]-[$\mathbf{Cu^{II}(HDO3A)}$] with apparent molar activities of 25−100 mCi/μmol at RT (Figure 8A,B). The corresponding complexes display excellent stability in phosphate-buffered saline buffer over the course of 15 h (Figure 8C), and [$\mathbf{^{64}Cu}$][$\mathbf{Cu^{II}(DO3A^{C4H8})}$] was stable for greater than 1 d in blood serum at pH 7.4 (Figure S27). Several independent studies have noted the propensity for DO3A-based conjugates to undergo transchelation with native proteins in vivo (e.g., superoxide dismutase, serum albumin, and metallothioneins).[32,33,151] Competitive transchelation challenges with a large excess of acyclic chelators (e.g., EDTA) with rapid transchelation kinetics have been used to probe this decomplexation pathway in vitro.[38,152−155] In the presence of 100-fold EDTA, [$\mathbf{^{64}Cu}$][$\mathbf{Cu^{II}(DO3A^{C4H8})}$] and [$\mathbf{^{64}Cu}$]-[$\mathbf{Cu^{II}(HDO3A)}$] were stable to transchelation over the course of 1 d at pH 5.5. Given that log β values for $\mathbf{Cu^{II}(DO3A^{C4H8})}$

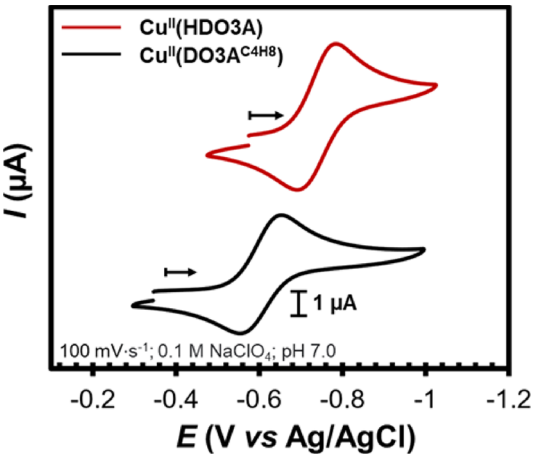

Figure 7. Cyclic voltammetry measurements of $\mathbf{Cu^{II}(HDO3A)}$ and $\mathbf{Cu^{II}(DO3A^{C4H8})}$ (pH 7, 0.1 M $NaClO_4$, and 100 mV/s).

https://doi.org/10.1021/acs.inorgchem.2c02907
Inorg. Chem. 2023, 62, 1362−1376

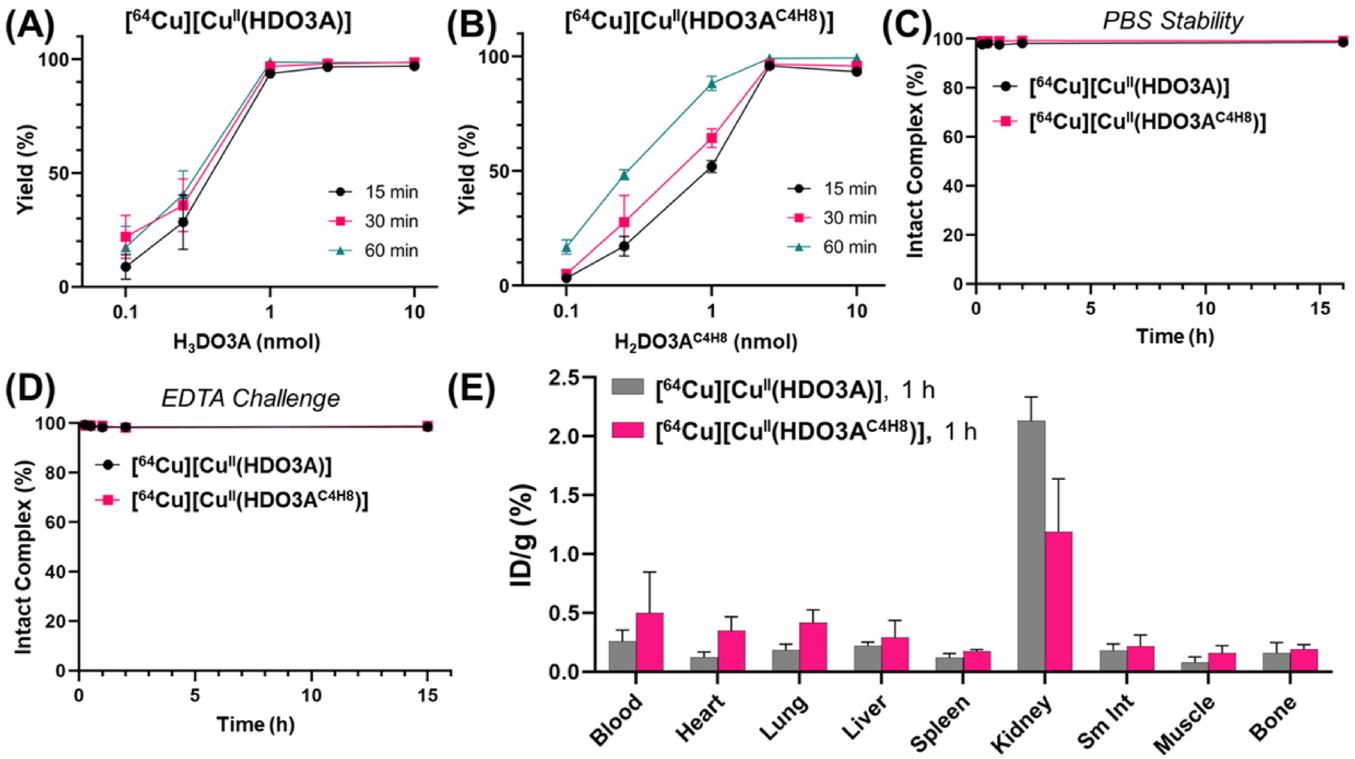

Figure 8. (A) Radiolabeling efficiency of H_3**DO3A**. (B) Radiolabeling efficiency of H_2**DO3A**^{C4H8}. (C) Time-dependent formulation stability of complexes in phosphate-buffered saline (PBS), pH 7.4, 25 °C. (D) Time-dependent stability of complexes (1.7 μM) in the presence of EDTA (1.7 mM) and NH_4OAc (41.7 mM), pH 5.5, 25 °C. (E) Biodistribution experiments (triplicate) 1 h after injection of either [^{64}**Cu**][**Cu**^{II}(**HDO3A**)] or [^{64}**Cu**][**Cu**^{II}(**DO3A**^{C4H8})].

are ∼2 orders of magnitude lower than Cu^{II}(EDTA) (Figure 8D; 18.46 vs 16.7),[156,157] this implicates significant kinetic stabilization of **Cu**^{II}(**DO3A**^{C4H8}) toward transchelation. This was unambiguously confirmed by transchelation studies performed on "cold" (^{nat}Cu) samples monitored by EPR spectroscopy at pH 7 ([Cu^{II}] = 1 mM). Over the course of 3 d, **Cu**^{II}(**DO3A**^{C4H8}) was impervious to transchelation with sevenfold excess Na_2EDTA at RT but proceeded quantitatively at 80 °C (Figure S9). While further studies are needed to delineate the structural effects contributing to the unexpected kinetic stability of **Cu**^{II}(**DO3A**^{C4H8}), our results suggest that *N*-protonation does not necessarily lead to inherently unstable/reactive species.

Next, we evaluated the stability of [^{64}**Cu**][**Cu**^{II}(**DO3A**^{C4H8})] and [^{64}**Cu**][**Cu**^{II}(**HDO3A**)] in vivo with biodistribution studies performed on male BALB/c mice intravenously injected with 0.7−1.3 MBq ^{64}Cu species via a tail-vein catheter (Figure 8E). Biodistribution studies performed 1 h after injection revealed low accumulation of [^{64}**Cu**]-[**Cu**^{II}(**HDO3A**)] and [^{64}**Cu**][**Cu**^{II}(**DO3A**^{C4H8})] in the liver and the blood. These initial results suggest comparable complex stability in vivo; however, more detailed metabolism studies are needed to fully establish the fate of ^{64}Cu being excreted and/or localized in organs/tissues.

■ CONCLUSIONS

In conclusion, we have reported the synthesis, characterization, and reactivity of a novel spirocyclic cyclen-based polyaminocarboxylate, H_2**DO3A**^{C4H8}, and its copper complex, **Cu**^{II}(**DO3A**^{C4H8}). These species serve as models of possible *N*-protonated intermediates of **Cu**^{II}(**HDO3A**), the parent structure of the FDA-approved radiopharmaceutical, [^{64}**Cu**]-[**Cu**^{II}(**DOTATATE**)], and several bifunctional chelators currently being explored in clinical trials. Our detailed experimental and computational studies helped resolve the pH-dependent speciation of **Cu**^{II}(**HDO3A**) and led to the isolation and characterization of an unprecedented *O*-protonated isomer of [**Cu**^{II}(H_2**DO3A**)]$^+$. Our reactivity studies demonstrated that both *N*-alkylated and *O*-protonated species were susceptible to (acid-mediated and reduction-induced) demetallation at low pH (<3) but displayed excellent stability under more physiologically relevant conditions. The *N*-protonated model, **Cu**^{II}(**DO3A**^{C4H8}) and [^{64}**Cu**]-[**Cu**^{II}(**DO3A**^{C4H8})], displayed unanticipated kinetic stability against direct transchelation with excess Na_2EDTA at RT, despite EDTA's rapid binding kinetics and higher stability constant (log β = 18.46 vs 16.7). Both [^{64}**Cu**]-[**Cu**^{II}(**DO3A**^{C4H8})] and [^{64}**Cu**][**Cu**^{II}(**HDO3A**)] displayed encouraging performance in vivo and suggest that alternative mechanisms for Cu-loss from **Cu**^{II}(**DO3A**^{C4H8}) and **Cu**^{II}(**HDO3A**) may prevail in vivo.

Looking forward, there remains a clear need to develop more robust in vitro assays to help benchmark and guide designs for stable ^{64}Cu agents. Similar to a growing number of reports,[37,38,40,134−136,138] our study reveals that several standard in vitro benchmarks for stability (e.g., acid-mediated dissociation, reductive-induced demetallation, and stability constants) were entirely inadequate to forecast the performance of these agents under more physiologically relevant conditions. *N*-protonated species of macrocyclic polyaminocarboxylates have been proposed as key reactive intermediates along the dissociation pathway;[92,94−107] however, the significant kinetic stability of **Cu**^{II}(**DO3A**^{C4H8}) toward transchelation and encouraging in vivo performance calls this into question.

https://doi.org/10.1021/acs.inorgchem.2c02907
Inorg. Chem. 2023, 62, 1362−1376

While *N,N*-alkylation leads to the lower stability of $Cu^{II}(DO3A^{C4H8})$ relative to $[Cu^{II}(DO3A)]^-$, key structural attributes (e.g., charge and constrained macrocyclic conformation) must contribute to the enhanced kinetic stability. Disambiguation of such effects is central to the development of critical structure−function relationships necessary to guide further chelator design. Further studies evaluating the properties and stability of *N*-alkylated conjugates and the use of *N,N*-spirocyclic ammonium as models for *N*-protonation of other macrocycles are ongoing.

EXPERIMENTAL SECTION

General Methods. *Materials.* Deuterated solvents were purchased from Cambridge Isotope Laboratories, Inc. Reagent-grade dichloromethane and acetone were purchased from Fisher Scientific. Anhydrous acetonitrile was obtained from HPLC-grade acetonitrile sparged for 20 min with dry Ar that was dried using a commercial two-column solvent purification system (LC Technologies). Reagent grade (70%) nitric acid was purchased from sigma Aldrich. Ultrapure, deionized water (18.2 MΩ) was obtained from a Millipore Direct-Q 3 UV Water Purification System. Cyclen (Carbosynth; 98%), 1,4-dibromobutane (Oakwood Chemicals; 99%), tert-butylbromoacetate (AK Scientific; 98%), K_2CO_3 (Fisher Chemical, Anhydrous, >99.0%, Certified ACS), $Cu(OAc)_2$ (Sigma Aldrich; 98%), and ethylenediaminetetraacetic acid (EDTA) disodium salt dihydrate (Sigma Aldrich; 99.0−101%) were obtained from commercial sources and used without further purification. $[^{OtBu}DO3A]Br$[158] and H_3DO3A[159] were synthesized according to previous literature procedures.

Synthesis and Characterization. Synthesis of 8,11,14-Tris(2-(tert-butoxy)-2-oxoethyl)-5,8,11,14-tetraazaspiro[4.11]hexadecan-5-ium ($[^{OtBu}DO3A^{C4H8}]Br$). A 200 mL round-bottom flask was charged with $[H\text{-}^{OtBu}DO3A]Br$ (5.06 g, 8.49 mmol, 1 equiv; MW: 595.62 g·mol^{-1}), acetonitrile (70 mL), and a Teflon-coated stir bar. Potassium carbonate (2.35 g, 17.03 mmol, 2 equiv; MW: 132.5 g·mol^{-1}) and 1,4-dibromobutane (2.54 mL, 21.27 mmol, 2.5 equiv; MW: 215.92 g·mol^{-1}) were added to the stirring colorless solution. The white slurry was heated in an oil bath at 70 °C for 24 h, where the solution gradually took on a yellow hue. After cooling to RT, the reaction was passed through a coarse-porosity fritted filter padded with Celite. The solvent was removed under reduced pressure (rotary evaporator) to furnish a yellow oil. The oil was dissolved in minimal dichloromethane (4 mL) and purified by column chromatography (SiO_2, 80:20 CH_2Cl_2/MeOH). The filtrate was collected, and solvents were removed under reduced pressure to isolate the product, $[^{OtBu}DO3A^{C4H8}]Br$, as a yellow tacky glass: 4.04 g (7.10 mmol, MW: 650.72 g·mol^{-1}, 72% yield). In one instance, X-ray diffraction quality crystals of $[H^{OtBu}DO3A^{C4H8}]Br_2$ could be produced from the crude product (no chromatographic purification) via slow evaporation of a concentrated CH_2Cl_2 solution (>100 mg/mL) at RT. ^{1}H NMR (400 MHz, $CDCl_3$, 298 K) δ: 1.32 (s, 9H, O^t*Bu*), 1.32 (s, 18H, O^t*Bu*), 2.12 (br, 4H, *spiro*-N$^+$CH$_2$C*H*$_2$), 2.53 (br, 4H, NCH$_2$C*H*$_2$), 2.60 (br, 4H, NC*H*$_2$CH$_2$), 3.10 (t, J = 5.4 Hz, 4H, *cyclen*-N$^+$CH$_2$C*H*$_2$), 3.15 (s, 2H, NC*H*$_2$COO$^-$), 3.20 (s, 4H NC*H*$_2$COO$^-$), 3.74 (t, J = 5.7 Hz, 4H, *spiro*-N$^+$C*H*$_2$CH$_2$), 3.81, (t, J = 5.5 Hz, 4H, *cyclen*-N$^+$C*H*$_2$CH$_2$), ^{13}C{^{1}H} NMR (101 MHz, $CDCl_3$, 298 K) δ: 21.3, 27.8, 48.6, 52.8, 53.7, 56.2, 56.8, 57.3, 62.7, 81.1, 81.4, 170.2, 170.6. IR: (ATR): 3350 (O−H, m br), 1714 (C═O, s), 1663 (C═O, s), 1487 (w), 1463 (w) 1416 (w), 1391 (w), 1351 (w), 1319 (w), 1284 (w), 1185 (m), 1164 (m), 1122 (m), 1089 (m), 1067 (m), 1049 (m), 997 (m), 969 (w), 946 (w), 898 (w), 829 (w), 798 (w), 719 (w), 675 (w), 599 (w), 574 (w), 551 (w), 476 (w), 445 (w), 405 (w). HRMS (ESI) m/z: $[M]^+$ calcd for $C_{30}H_{57}N_4O_6$: 567.4122; found: 567.4109.

Synthesis of 2-(8,14-Bis(carboxymethyl)-5,8,11,14-tetraazaspiro[4.11]hexadecan-5-ium-11-yl)acetate (H_2DO3A^{C4H8}). A 200 mL round-bottom flask was charged with $[H\text{-}^{OtBu}DO3A]Br$ (5.00 g, 8.4 mmol, 1 equiv; MW: 595.62 g·mol^{-1}), acetonitrile (70 mL), and a Teflon-coated stir bar. Potassium carbonate (2.32 g, 17.50 mmol, 2 equiv; MW: 132.5 g·mol^{-1}) and 1,4-dibromobutane (1.09 mL, 9.130 mmol, 1.10 equiv; MW: 215.92 g·mol^{-1}) were added to the stirring colorless solution. The white slurry was heated in an oil bath at 70 °C for 24 h, where the solution gradually took on a yellow hue. After cooling to RT, the reaction was passed through a coarse-porosity fritted filter padded with Celite and the solvent was removed under reduced pressure (rotary evaporator, Schlenk line) to furnish a light brown solid. The solid was dissolved in a minimal amount of dichloromethane (15 mL), and a Teflon-coated stir bar was added. TFA (30 mL) was added over the course of 10 min to the stirring light-yellow solution resulting in a color change to dark yellow. The mixture was stirred for 12 h at RT before solvents were removed under reduced pressure (Schlenk line, external trap) to form a brown oil. The exact concentration of the product and total amount of trifluoroacetate and TFA were determined through quantitative ^{1}H NMR and ^{19}F NMR spectroscopy using potassium hydrogen phthalate and potassium hexafluorophosphate as internal standards, respectively. The brown oil was dissolved in a minimal amount of acetonitrile (30 mL) and triethylamine (2.90 g, 28.7 mmol, 3.4 equiv, 1:1 NEt_3/TFA & TFA$^-$; MW: 101.19 g·mol^{-1}) was added over the course of 5 min to form a light-brown precipitate. The solution was stirred for 1 h at RT. The precipitate was isolated on a medium-porosity fritted filter, washed with acetonitrile (60 mL), and dried under reduced pressure (Schlenk line, 50 mTorr) to isolate the product, H_2DO3A^{C4H8}, as a white powder. 1.50 g (3.75 mmol, 45% yield; MW: 400.47 g·mol^{-1}).

Note: After establishing an accurate molecular weight from ^{1}H NMR and ^{19}F NMR, the material can be used for metalation reactions without further purification. **Note**: In one instance, X-ray diffraction quality crystals of $[H_3DO3A^{C4H8}]Cl\bullet 3H_2O$ were produced upon layering a 100 mg/mL aqueous solution of H_2DO3A^{C4H8} (lowered to pH ≤ 2 with HCl) with acetone (∼2:1). ^{1}H NMR (400 MHz, D_2O, 298 K, pH 9.0): δ = 2.21 (m, 4H; *spiro*-N$^+$CH$_2$C*H*$_2$), 2.97 (t, J = 4.9 Hz, *cyclen*-N$^+$CH$_2$C*H*$_2$), 3.14 (t, J = 5.9 Hz, 4H; NCH$_2$C*H*$_2$), 3.27 (br, 8H; NC*H*$_2$CH$_2$ + NC*H*$_2$COOH), 3.57 (t, J = 6.6 Hz, 4H; *spiro*-N$^+$CH$_2$C*H*$_2$), 3.61 (s, 2H; NC*H*$_2$COO$^-$), 3.81(t, J = 5.8 Hz, 4H; *cyclen*-N$^+$C*H*$_2$CH$_2$),^{13}C{^{1}H} NMR (101 MHz, D_2O, 298 K, pH 9.0): δ = 21.5, 47.9, 50.0, 51.5, 57.1, 58.2, 58.3, 64.1, 174.0, 178.8. IR: (ATR): 3350 (O−H, m br), 1714 (C═O, s), 1663 (C═O, s), 1487 (w), 1463 (w) 1416 (w), 1391 (w), 1351 (w), 1319 (w), 1284 (w), 1185 (m), 1164 (m), 1122 (m), 1089 (m), 1067 (m), 1049 (m), 997 (m), 969 (w), 946 (w), 898 (w), 829 (w), 798 (w), 719 (w), 675 (w), 599 (w), 574 (w), 551 (w), 476 (w), 445 (w), 405 (w); HRMS (ESI) m/z: $[M]^+$ calcd for $C_{18}H_{34}N_4O_6$ 402.2478; found: 402.2448.

Synthesis of $Cu^{II}(DO3A^{C4H8})$. A 20 mL scintillation vial was charged with H_2DO3A^{C4H8} (250.0 mg, 0.624 mmol, 1 equiv; MW: 400.47 g·mol^{-1}), a Teflon-coated stir bar, and water (3 mL). Copper acetate (94.3 mg, 0.520 mmol, 1 equiv; MW: 181.63 g·mol^{-1}) was added to the stirring colorless solution. The clear blue solution was stirred for 24 h at RT. After this time, the stir bar was removed, and the solution was layered with acetone (6 mL). Blue crystals were formed after 12−24 h at RT, isolated by filtration over a medium-porosity fritted filter, and dried under reduced pressure to yield the product, $Cu^{II}(DO3A^{C4H8})$. 235.0 mg (0.509 mmol, 76% yield; MW: 462.01 g·mol^{-1}) IR: (ATR): 3373 (O−H, m, br), 1643 (m), 1587 (C═O, s), 1481 (w), 1428 (w), 1424 (w), 1333 (m, br), 1176 (w), 1134 (w), 1147 (w), 1078 (w), 1064 (m), 1061 (m), 1035 (w), 990 (m), 982 (w), 936 (m), 920 (m), 906 (m), 871 (m), 818 (m), 777 (w), 734 (m), 700 (m), 627 (m), 556 (m) cm^{-1}; elemental analysis calcd (%) for $C_{18}H_{30}N_4O_6Cu\cdot(H_2O)_4$: C 40.48, H 7.17, N 10.49; found: C 40.83, H 7.19, N 10.39. HRMS (ESI) m/z: $[M + H]^+$ calcd for $C_{18}H_{31}N_4O_6Cu$: 462.1534; found: 462.1528.

Synthesis of $Cu^{II}(HDO3A)$. **Note**: $Cu^{II}(HDO3A)$ was synthesized with slight modifications to the literature procedure.[158] A 20 mL scintillation vial was charged with H_3DO3A (384.0 mg, 1.11 mmol, 1 equiv; MW: 346.38 g·mol^{-1}), a Teflon-coated stir bar, and water (3 mL). Copper acetate (201.6 mg, 1.11 mmol, 1 equiv; MW: 181.63 g·mol^{-1}) was added to the stirring colorless solution. The resulting blue solution was stirred for 24 h at RT. After this time, the stir bar was removed, the pH was adjusted to 7.0 through dropwise addition of 0.1

https://doi.org/10.1021/acs.inorgchem.2c02907
Inorg. Chem. 2023, 62, 1362−1376

M sodium hydroxide, and the solution was concentrated to ~500 μL under reduced pressure. The dark blue solution was layered with ether and allowed to sit undisturbed overnight. The light-green precipitate was isolated, dried under reduced pressure, and redissolved in a minimal amount of methanol (~2 mL). The product was then re-precipitated with excess ether (~5 mL). The solution was allowed to sit undisturbed at 0 °C overnight to yield the product, **Cu^{II}(HDO3A)**, as a light green powder (348.0 mg, 0.853 mmol, 77% yield; MW: 407.91 g·mol^{-1}). IR: (ATR, Cu(HDO3A)): 3218 (w), 2966 (w), 2924 (w), 2861 (w), 1716 (C═O, m) 1632 (C═O, s), 1573 (C═O, s), 1455 (w), 1439 (w), 1409 (w), 1395 (w), 1359 (s), 1327 (m), 1239 (w), 1088 (m), 1045 (w), 991 (w), 956 (m), 926 (m), 910 (m), 874 (w), 831 (w), 804 (m), 780 (w), 727 (w), 696 (m), 626 (s) 573 (w).

[Cu^{II}(H_2DO3A)]Br. A 4 mL vial was charged with **Cu^{II}(HDO3A)** (50.0 mg, 0.126 mmol, 1 equiv; MW: 407.91 g·mol^{-1}) and dissolved in water (0.5 mL). Ammonium bromide (120.0 mg, 1.225 mmol, 10 equiv; MW: g·mol^{-1}g/mol) was dissolved in the solution, and the pH was adjusted to ~3 through dropwise addition of hydrochloric acid. The solution was then layered in acetone. Over a period of ~1 week, **[Cu(H_2DO3A)]Br·(H_2O)$_{0.5}$** precipitated as light blue crystals (22.0 mg, 0.042 mmol, 34% yield; 505.83 g·mol^{-1}g/mol). IR: (ATR, **[Cu(H_2DO3A)]Br·(H_2O)$_{0.5}$**): 2882 (O−H, m br), 1722 (C═O, s), 1662 (C═O, s), 1594 (C═O, s), 1464 (w) 1403 (w), 1348 (w), 1173 (s), 1125 (s), 1073 (s), 970 (w), 922 (w), 898 (w), 881 (w), 826 (w), 796 (m), 717 (m), 680 (w); elemental analysis calcd (%) for $C_{14}H_{25}BrCuN_4O_6 \cdot (H_2O)_{0.5}$: C 33.78, H 5.26, N 11.25; found: C 33.73, H 5.29, N 11.10.

Instruments and Measurements. Unless specified, all reactions were performed under an ambient atmosphere. Unless specified, ultrapure, deionized water (18.2 MΩ; Millipore) was used for all reactions and measurements. Glassware was oven-dried for at least 2 h at 150 °C prior to use. The following spectrometers were used for NMR characterization: a Bruker Avance III HD Ascend (^{1}H: 600 MHz, ^{13}C: 152 MHz) and a Bruker DRX (^{1}H: 400 MHz, ^{13}C: 101 MHz). ^{1}H and ^{13}C NMR shifts for samples run in $CDCl_3$ are referenced relative to the solvent signal ($CDCl_3$: ^{1}H: 7.26 ppm, ^{13}C: 77.16 ppm), samples run in D_2O are referenced relative to the solvent signal and external solution standards (D_2O: ^{1}H: 4.79, triethylamine: ^{13}C: 47.19 ppm, methyl tertbutyl ether ^{13}C: 27.9 ppm). UV−vis absorption spectroscopy was performed with a Cary 8454 spectrometer. Mass spectra were obtained on an Agilent 6530 LC−MS utilizing electrospray ionization and quadrupole time of flight detection. Infrared spectra were recorded on powder samples using a Jasco FT/IR-4100 spectrometer. Elemental analyses were performed by Robertson Microlit Laboratories (Ledgewood, NJ) and/or Midwest Microlab, LLC (Indianapolis, IN).

X-ray Crystallography. Samples were removed from the mother liquor, rinsed with acetone, and then transferred covered in Paraton oil to a glass slide where it was evaluated and mounted with the assistance of an optical microscope. X-ray reflection intensity data were collected on a Bruker D8 Quest with a Photon 100 CMOS detector employing graphite-monochromated Mo-Kα radiation (λ = 0.71073 Å) at a temperature of 173(1) K. Rotation frames were integrated using SAINT,[4] producing a listing of unaveraged F^2 and $\sigma(F^2)$ values, which were then passed to the SHELXT[5] program package for further processing and structure solution. The intensity data were corrected for Lorentz and polarization effects and for absorption using SADABS.[6] The structures were solved by direct methods (SHELXT).[5] Refinement was by full-matrix least squares based on F^2 using SHELXL.[7] All reflections were used during refinements. Non-hydrogen atoms were refined anisotropically, and hydrogen atoms were refined using a riding model. In **[^{tBu}DO3A^{C4H8}]Br_2•H_2O,2CH_2Cl_2**, one molecule of CH_2Cl_2 was found to be disordered over two positions, and H-atoms were not assigned for the one water molecule (O7) due to issues with reliable placement from the difference map (the two H-atoms were still included in the formula). In the case of **[H_3DO3A^{C4H8}]Cl•3H_2O**, both O(4) and O(6) are homoconjugated with O(4)′ and O(6)′ over a special position (net charge balance of the carboxylate/carboxylic acid groups: two carboxylic acids and one carboxylate). In the case of **Cu(DO3A^{C4H8})**, two water molecules (O9 and O10) were found to be disordered over two positions.

EPR Spectroscopy. EPR spectra were collected on a Bruker EMX Premium-X spectrometer with a field strength of 9.65 GHz and a microwave power of 2.0 mW at 77 K using a liquid-nitrogen finger dewar (Wilmad, 50 mL Suprasil). Sample solutions (~10 mM) were prepared as 50:50 V/V solutions in deionized water/ethylene glycol with 100 mM sodium perchlorate. All samples were degassed with nitrogen and placed in 4-mm o.d. quartz EPR tubes. Samples were glassed by slowly lowering the sample into liquid nitrogen (~2 mm s^{-1}). The experimental spectra were simulated using EasySpin.[2] In all cases, a representative fit was achieved through the use of the Nelder/Mead simplex model or Levenberg/Marquardt algorithm while assuming isotropic line broadening.

Potentiometric Titrations. Potentiometric measurements were performed using a Metrohm 916 Ti-touch autotitrator equipped with a Metrohm unitrode electrode. Solutions of sodium hydroxide and nitric acid were prepared from boiled deionized water and blanketed under nitrogen. NaOH solutions were standardized against aspartic acid. The nitric acid concentration and percent carbonate impurity were established using Gran's method. The solution temperature was maintained at 25 ± 2 °C. In a typical titration, the desired analyte (~0.05 mmol; 100 mM $NaNO_3$) was titrated with a standardized solution of NaOH (0.200 M) at 25 °C. The ligand to metal ratio was held at 1.25:1, and 80−120 data points were obtained. Solutions were back-titrated with standardized solutions of HNO_3 (0.200 M) to confirm that equilibria were reached. To provide additional validation, titrations were repeated in the presence of 0.05 mM disodium EDTA (1.25:1:1 ratio of H_2DO3A^{C4H8} to metal to EDTA). Each titration was performed in triplicate, and all pK_a and log(β) values are averages of triplicate data that were fit using HyperQuad.[160] Speciation curves for the ligands and metal complexes were constructed from these values using HyperSpec.[161] Log(β) values for Cu^{II} and DO3A^{C4H8} were determined by holding the pK_a values of H_2DO3A^{C4H8}, the pK_a values of H_4EDTA (pK_{a1} = 10.24, pK_{a2} = 6.16, pK_{a3} = 2.66, pK_{a4} = 2.0, pK_{a5} = 1.5, and pK_{a5} = 0.0), and the log(β) values of Cu(EDTA) (log(β) = 18.46) constant while minimizing residuals through variation of the log(β) of Cu(DO3A^{C4H8}).[157] Fits with calculated residuals are provided in the Supporting Information (Figures S17 and S18).

Cyclic Voltammetry. Cyclic voltammetry measurements were performed using a CH730E Electrochemical Analyzer/Workstation, and the data were processed using CHI software version 12.04. Experiments were performed with deoxygenated aqueous solutions blanketed with a nitrogen atmosphere in a 10 mL glass cell using an Ag/AgCl (saturated KCl) reference electrode, glassy carbon working electrode, and platinum counter electrode. Prior to each experiment, the working electrode was polished for 60 s in a figure-eight motion on a microcloth polishing pad with 0.05 μm alumina powder and rinsed with deionized water. Typical measurements were performed on 2 mM analyte using 100 mM $NaClO_4$ as the supporting electrolyte. All potentials are not only reported with respect to the Ag/AgCl reference electrode but also referenced externally to a water-soluble ferrocene derivative, ferrocenemethanol [Fe^{II}($C_5H_4CH_2OH$)(C_5H_5)].[162,163]

Computational Methods. All calculations were performed employing the Gaussian 09 package (revision D.01).[10] Geometries were optimized at the M06-L level of theory[126] with Grimme's D3 dispersion correction,[11] using the Stuttgart [8s7p6d2f1g| 6s5p3d2f1g] ECP10MWB contracted pseudopotential basis set on copper[164] and the 6-31G(d′,p′) basis set on all other atoms.[165,166] Solvation effects associated with water were accounted for by using the SMD continuum solvation model.[167] Optimized geometries were confirmed as minima by frequency analysis (the absence of negative frequencies). To validate the selected methodology, the mean unsigned error (MUE) between the predicted and the experimentally determined (SC-XRD) bond lengths in the primary coordination sphere of **Cu^{II}(DO3A^{C4H8})** (MUE = 0.036), **Cu^{II}(HDO3A)** (MUE =

https://doi.org/10.1021/acs.inorgchem.2c02907
Inorg. Chem. 2023, 62, 1362−1376

0.107), and $[Cu^{II}(H_2DO3A)]^+$ (MUE = 0.067) were calculated by the following equation.

$$\mathrm{MUE} = \frac{\sum_{i=1}^{n} |y_i - x_i|}{n}$$

■ ASSOCIATED CONTENT

Supporting Information

The Supporting Information is available free of charge at https://pubs.acs.org/doi/10.1021/acs.inorgchem.2c02907.

Experimental procedures, additional figures, and tables (PDF)

Accession Codes

CCDC 2171218−2171220 and 2201225 contain the supplementary crystallographic data for this paper. These data can be obtained free of charge via www.ccdc.cam.ac.uk/data_request/cif, or by emailing data_request@ccdc.cam.ac.uk, or by contacting The Cambridge Crystallographic Data Centre, 12 Union Road, Cambridge CB2 1EZ, UK; fax: +44 1223 336033.

■ AUTHOR INFORMATION

Corresponding Authors

Eszter Boros − *Department of Chemistry, Stony Brook University, Stony Brook, New York 11794, United States;* orcid.org/0000-0002-4186-6586; Email: eszter.boros@stonybrook.edu

Jerome R. Robinson − *Department of Chemistry, Brown University, Providence, Rhode Island 02912, United States;* orcid.org/0000-0002-9111-3822; Email: Jerome_robinson@brown.edu

Authors

Alexander M. Brown − *Department of Chemistry, Brown University, Providence, Rhode Island 02912, United States*

Jana L. Butman − *Department of Chemistry, Brown University, Providence, Rhode Island 02912, United States*

Raphael Lengacher − *Department of Chemistry, Stony Brook University, Stony Brook, New York 11794, United States*

Natasha P. Vargo − *Department of Chemistry, Brown University, Providence, Rhode Island 02912, United States;* orcid.org/0000-0002-3907-3843

Kirsten E. Martin − *Department of Chemistry, Stony Brook University, Stony Brook, New York 11794, United States*

Angus Koller − *Department of Chemistry, Stony Brook University, Stony Brook, New York 11794, United States*

Dariusz Śmiłowicz − *Department of Chemistry, Stony Brook University, Stony Brook, New York 11794, United States*

Complete contact information is available at: https://pubs.acs.org/10.1021/acs.inorgchem.2c02907

Notes

The authors declare no competing financial interest.

■ ACKNOWLEDGMENTS

J.R.R. and A.M.B. gratefully acknowledge Brown University and the National Science Foundation (CHE-1900248) for funding. E.B. and R.L. acknowledge Stony Brook University for funding. J.R.R. thanks Dr. Patrick J. Carroll and Dr. Michael Gau for their helpful discussions.

■ REFERENCES

(1) Etzioni, R.; Urban, N.; Ramsey, S.; McIntosh, M.; Schwartz, S.; Reid, B.; Radich, J.; Anderson, G.; Hartwell, L. The case for early detection. *Nat. Rev. Cancer* **2003**, *3*, 243−252.

(2) Ott, J. J.; Ullrich, A.; Miller, A. B. The importance of early symptom recognition in the context of early detection and cancer survival. *Eur. J. Cancer* **2009**, *45*, 2743−2748.

(3) Thomson, C. S.; Forman, D. Cancer survival in England and the influence of early diagnosis: what can we learn from recent EUROCARE results? *Br. J. Cancer* **2009**, *101*, S102−S109.

(4) Yordanova, A.; Eppard, E.; Kürpig, S.; Bundschuh, R. A.; Schönberger, S.; Gonzalez-Carmona, M.; Feldmann, G.; Ahmadzadehfar, H.; Essler, M. Theranostics in nuclear medicine practice. *Onco Targets Ther.* **2017**, *10*, 4821−4828.

(5) Svenson, S. Theranostics: Are We There Yet? *Mol. Pharmaceutics* **2013**, *10*, 848−856.

(6) Taïeb, D.; Hicks, R. J.; Pacak, K. Nuclear Medicine in Cancer Theranostics: Beyond the Target. *J. Nucl. Med.* **2016**, *57*, 1659−1660.

(7) Fujibayashi, Y.; Matsumoto, K.; Yonekura, Y.; Konishi, J.; Yokoyama, A. A New Zinc-62/Copper-62 Generator as a Copper-62 Source for PET Radiopharmaceuticals. *J. Nucl. Med.* **1989**, *30*, 1838.

(8) Anderson, C. J.; Ferdani, R. Copper-64 radiopharmaceuticals for PET imaging of cancer: advances in preclinical and clinical research. *Cancer Biother. Radiopharm.* **2009**, *24*, 379−393.

(9) Paterson, B. M.; Donnelly, P. S.Macrocyclic Bifunctional Chelators and Conjugation Strategies for Copper-64 Radiopharmaceuticals. In *Advances in Inorganic Chemistry*, van Eldik, R.; Hubbard, C. D., Eds.; Academic Press, 2016; Vol. *68*, pp 223−251.

(10) Rowshanfarzad, P.; Sabet, M.; Jalilian, A. R.; Kamalidehghan, M. An overview of copper radionuclides and production of 61Cu by proton irradiation of (nat)Zn at a medical cyclotron. *Appl. Radiat. Isot.* **2006**, *64*, 1563−1573.

(11) Jones-Wilson, T. M.; Deal, K. A.; Anderson, C. J.; McCarthy, D. W.; Kovacs, Z.; Motekaitis, R. J.; Sherry, A. D.; Martell, A. E.; Welch, M. J. The in vivo behavior of copper-64-labeled azamacrocyclic complexes. *Nucl. Med. Biol.* **1998**, *25*, 523−530.

(12) Boschi, A.; Martini, P.; Janevik-Ivanovska, E.; Duatti, A. The emerging role of copper-64 radiopharmaceuticals as cancer theranostics. *Drug Discovery Today* **2018**, *23*, 1489−1501.

(13) Ahmedova, A.; Todorov, B.; Burdzhiev, N.; Goze, C. Copper radiopharmaceuticals for theranostic applications. *Eur. J. Med. Chem.* **2018**, *157*, 1406−1425.

(14) Novak-Hofer, I.; Schubiger, A. P. Copper-67 as a therapeutic nuclide for radioimmunotherapy. *Eur. J. Nucl. Med. Mol. Imaging* **2002**, *29*, 821−830.

(15) Cai, Z.; Anderson, C. J. Chelators for copper radionuclides in positron emission tomography radiopharmaceuticals. *J. Labelled Compd. Radiopharm.* **2014**, *57*, 224−230.

(16) Knighton, R. C.; Troadec, T.; Mazan, V.; Le Saëc, P.; Marionneau-Lambot, S.; Le Bihan, T.; Saffon-Merceron, N.; Le Bris, N.; Chérel, M.; Faivre-Chauvet, A.; Elhabiri, M.; Charbonnière, L. J.; Tripier, R. Cyclam-Based Chelators Bearing Phosphonated Pyridine Pendants for 64Cu-PET Imaging: Synthesis, Physicochemical Studies, Radiolabeling, and Bioimaging. *Inorg. Chem.* **2021**, *60*, 2634.

(17) Huang, Y.; Huynh, T. T.; Sun, L.; Hu, C.-H.; Wang, Y.-C.; Rogers, B. E.; Mirica, L. M. Neutral Ligands as Potential 64Cu Chelators for Positron Emission Tomography Imaging Applications in Alzheimer's Disease. *Inorg. Chem.* **2022**, *61*, 4778−4787.

(18) Andersen, T. L.; Baun, C.; Olsen, B. B.; Dam, J. H.; Thisgaard, H. Improving Contrast and Detectability: Imaging with [(55)Co]Co-DOTATATE in Comparison with [(64)Cu]Cu-DOTATATE and [(68)Ga]Ga-DOTATATE. *J. Nucl. Med.* **2020**, *61*, 228−233.

(19) Dai, L.; Zhang, J.; Wong, C. T.; Chan, W. T. K.; Ling, X.; Anderson, C. J.; Law, G.-L. Design of Functional Chiral Cyclen-Based Radiometal Chelators for Theranostics. *Inorg. Chem.* **2021**, *60*, 7082.

(20) Benešová, M.; Schäfer, M.; Bauder-Wüst, U.; Afshar-Oromieh, A.; Kratochwil, C.; Mier, W.; Haberkorn, U.; Kopka, K.; Eder, M. Preclinical Evaluation of a Tailor-Made DOTA-Conjugated PSMA

Inhibitor with Optimized Linker Moiety for Imaging and Endoradiotherapy of Prostate Cancer. *J. Nucl. Med.* **2015**, *56*, 914−920.
(21) Alirezapour, B.; Rasaee, M. J.; Jalilian, A. R.; Rajabifar, S.; Mohammadnejad, J.; Paknejad, M.; Maadi, E.; Moradkhani, S. Development of [64Cu]-DOTA-PR81 radioimmunoconjugate for MUC-1 positive PET imaging. *Nucl. Med. Biol.* **2016**, *43*, 73−80.
(22) Kostelnik, T. I.; Orvig, C. Radioactive Main Group and Rare Earth Metals for Imaging and Therapy. *Chem. Rev.* **2019**, *119*, 902−956.
(23) https://www.clinicaltrials.gov/ (accessed April 4).
(24) Pfeifer, A.; Knigge, U.; Binderup, T.; Mortensen, J.; Oturai, P.; Loft, A.; Berthelsen, A. K.; Langer, S. W.; Rasmussen, P.; Elema, D.; Von Benzon, E.; Højgaard, L.; Kjaer, A. 64Cu-DOTATATE PET for Neuroendocrine Tumors: A Prospective Head-to-Head Comparison with 111In-DTPA-Octreotide in 112 Patients. *J. Nucl. Med.* **2015**, *56*, 847−854.
(25) Johnbeck, C. B.; Knigge, U.; Loft, A.; Berthelsen, A. K.; Mortensen, J.; Oturai, P.; Langer, S. W.; Elema, D. R.; Kjaer, A. Head-to-Head Comparison of 64Cu-DOTATATE and 68Ga-DOTATOC PET/CT: A Prospective Study of 59 Patients with Neuroendocrine Tumors. *J. Nucl. Med.* **2017**, *58*, 451−457.
(26) Pfeifer, A.; Knigge, U.; Mortensen, J.; Oturai, P.; Berthelsen, A. K.; Loft, A.; Binderup, T.; Rasmussen, P.; Elema, D.; Klausen, T. L.; Holm, S.; Von Benzon, E.; Højgaard, L.; Kjaer, A. Clinical PET of Neuroendocrine Tumors Using ^{64}Cu-DOTATATE: First-in-Humans Study. *J. Nucl. Med.* **2012**, *53*, 1207−1215.
(27) Kumar, S. R.; Gallazzi, F. A.; Ferdani, R.; Anderson, C. J.; Quinn, T. P.; Deutscher, S. L. In vitro and in vivo evaluation of ^{64}Cu-radiolabeled KCCYSL peptides for targeting epidermal growth factor receptor-2 in breast carcinomas. *Cancer Biother. Radiopharm.* **2010**, *25*, 693−703.
(28) Wu, N.; Kang, C. S.; Sin, I.; Ren, S.; Liu, D.; Ruthengael, V. C.; Lewis, M. R.; Chong, H. S. Promising bifunctional chelators for copper 64-PET imaging: practical (64)Cu radiolabeling and high in vitro and in vivo complex stability. *J. Biol. Inorg. Chem.* **2016**, *21*, 177−184.
(29) Ait-Mohand, S.; Fournier, P.; Dumulon-Perreault, V.; Kiefer, G. E.; Jurek, P.; Ferreira, C. L.; Bénard, F.; Guérin, B. Evaluation of 64Cu-Labeled Bifunctional Chelate−Bombesin Conjugates. *Bioconjugate Chem.* **2011**, *22*, 1729−1735.
(30) Park, J.-A.; Lee, J. W.; Kim, H.-K.; Shin, U. C.; Lee, K. C.; Kim, T.-J.; Chang, Y.; Kim, K. M.; Kim, J. Y.; Lee, Y. J. Radiometallic Complexes of DO3A-Benzothiazole Aniline for Nuclear Medicine Theranostics. *Mol. Pharmaceutics* **2018**, *15*, 1133−1141.
(31) Banerjee, S. R.; Pullambhatla, M.; Foss, C. A.; Nimmagadda, S.; Ferdani, R.; Anderson, C. J.; Mease, R. C.; Pomper, M. G. 64Cu-Labeled Inhibitors of Prostate-Specific Membrane Antigen for PET Imaging of Prostate Cancer. *J. Med. Chem.* **2014**, *57*, 2657−2669.
(32) Boswell, C. A.; Sun, X.; Niu, W.; Weisman, G. R.; Wong, E. H.; Rheingold, A. L.; Anderson, C. J. Comparative in Vivo Stability of Copper-64-Labeled Cross-Bridged and Conventional Tetraazamacrocyclic Complexes. *J. Med. Chem.* **2004**, *47*, 1465−1474.
(33) Ping Li, W.; Meyer, L. A.; Capretto, D. A.; Sherman, C. D.; Anderson, C. J. Receptor-Binding, Biodistribution, and Metabolism Studies of 64Cu-DOTA-Cetuximab, a PET-Imaging Agent for Epidermal Growth-Factor Receptor-Positive Tumors. *Cancer Biother. Radiopharm.* **2008**, *23*, 158−171.
(34) Kubíček, V.; Böhmová, Z.; Ševčíková, R.; Vaněk, J.; Lubal, P.; Poláková, Z.; Michalicová, R.; Kotek, J.; Hermann, P. NOTA Complexes with Copper(II) and Divalent Metal Ions: Kinetic and Thermodynamic Studies. *Inorg. Chem.* **2018**, *57*, 3061−3072.
(35) Voráčová, I.; Vaněk, J.; Pasulka, J.; Střelcová, Z.; Lubal, P.; Hermann, P. Dissociation kinetics study of copper(II) complexes of DO3A, DOTA and its monosubstituted derivatives. *Polyhedron* **2013**, *61*, 99−104.
(36) Lubal, P.; Kývala, M. R.; Hermann, P.; Holubová, J.; Rohovec, J.; Havel, J.; Lukeš, I. Thermodynamic and kinetic study of copper(II) complexes with N-methylene(phenylphosphinic acid) derivatives of cyclen and cyclam. *Polyhedron* **2001**, *20*, 47−55.
(37) Woodin, K. S.; Heroux, K. J.; Boswell, C. A.; Wong, E. H.; Weisman, G. R.; Niu, W.; Tomellini, S. A.; Anderson, C. J.; Zakharov, L. N.; Rheingold, A. L. Kinetic Inertness and Electrochemical Behavior of Copper(II) Tetraazamacrocyclic Complexes: Possible Implications for in Vivo Stability. *Eur. J. Inorg. Chem.* **2005**, *2005*, 4829−4833.
(38) Vaughn, B. A.; Brown, A. M.; Ahn, S. H.; Robinson, J. R.; Boros, E. Is Less More? Influence of the Coordination Geometry of Copper(II) Picolinate Chelate Complexes on Metabolic Stability. *Inorg. Chem.* **2020**, *59*, 16095−16108.
(39) Tosato, M.; Dalla Tiezza, M.; May, N. V.; Isse, A. A.; Nardella, S.; Orian, L.; Verona, M.; Vaccarin, C.; Alker, A.; Mäcke, H.; Pastore, P.; Di Marco, V. Copper Coordination Chemistry of Sulfur Pendant Cyclen Derivatives: An Attempt to Hinder the Reductive-Induced Demetalation in 64/67Cu Radiopharmaceuticals. *Inorg. Chem.* **2021**, *60*, 11530.
(40) Uzal-Varela, R.; Patinec, V.; Tripier, R.; Valencia, L.; Maneiro, M.; Canle, M.; Platas-Iglesias, C.; Esteban-Gómez, D.; Iglesias, E. On the dissociation pathways of copper complexes relevant as PET imaging agents. *J. Inorg. Biochem.* **2022**, *236*, No. 111951.
(41) Price, E. W.; Orvig, C. Matching chelators to radiometals for radiopharmaceuticals. *Chem. Soc. Rev.* **2014**, *43*, 260−290.
(42) Sarkar, S.; Bhatt, N.; Ha, Y. S.; Huynh, P. T.; Soni, N.; Lee, W.; Lee, Y. J.; Kim, J. Y.; Pandya, D. N.; An, G. I.; Lee, K. C.; Chang, Y.; Yoo, J. High in Vivo Stability of 64Cu-Labeled Cross-Bridged Chelators Is a Crucial Factor in Improved Tumor Imaging of RGD Peptide Conjugates. *J. Med. Chem.* **2018**, *61*, 385−395.
(43) Sun, X.; Wuest, M.; Weisman, G. R.; Wong, E. H.; Reed, D. P.; Boswell, C. A.; Motekaitis, R.; Martell, A. E.; Welch, M. J.; Anderson, C. J. Radiolabeling and In Vivo Behavior of Copper-64-Labeled Cross-Bridged Cyclam Ligands. *J. Med. Chem.* **2002**, *45*, 469−477.
(44) Boswell, C. A.; McQuade, P.; Weisman, G. R.; Wong, E. H.; Anderson, C. J. Optimization of labeling and metabolite analysis of copper-64-labeled azamacrocyclic chelators by radio-LC-MS. *Nucl. Med. Biol.* **2005**, *32*, 29−38.
(45) Wadas, T. J.; Anderson, C. J. Radiolabeling of TETA- and CB-TE2A-conjugated peptides with copper-64. *Nat. Protoc.* **2006**, *1*, 3062−3068.
(46) Bhatt, N.; Soni, N.; Ha, Y. S.; Lee, W.; Pandya, D. N.; Sarkar, S.; Kim, J. Y.; Lee, H.; Kim, S. H.; An, G. I.; Yoo, J. Phosphonate Pendant Armed Propylene Cross-Bridged Cyclam: Synthesis and Evaluation as a Chelator for Cu-64. *ACS Med. Chem. Lett.* **2015**, *6*, 1162−1166.
(47) Lima, L. M. P.; Esteban-Gómez, D.; Delgado, R.; Platas-Iglesias, C.; Tripier, R. Monopicolinate Cyclen and Cyclam Derivatives for Stable Copper(II) Complexation. *Inorg. Chem.* **2012**, *51*, 6916−6927.
(48) Lima, L. M. P.; Halime, Z.; Marion, R.; Camus, N.; Delgado, R.; Platas-Iglesias, C.; Tripier, R. Monopicolinate Cross-Bridged Cyclam Combining Very Fast Complexation with Very High Stability and Inertness of Its Copper(II) Complex. *Inorg. Chem.* **2014**, *53*, 5269−5279.
(49) Rylova, S. N.; Stoykow, C.; Del Pozzo, L.; Abiraj, K.; Tamma, M. L.; Kiefer, Y.; Fani, M.; Maecke, H. R. The somatostatin receptor 2 antagonist 64Cu-NODAGA-JR11 outperforms 64Cu-DOTA-TATE in a mouse xenograft model. *PLoS One* **2018**, *13*, No. e0195802.
(50) Guillou, A.; Lima, L. M. P.; Roger, M.; Esteban-Gómez, D.; Delgado, R.; Platas-Iglesias, C.; Patinec, V.; Tripier, R. 1,4,7-Triazacyclononane-Based Bifunctional Picolinate Ligands for Efficient Copper Complexation. *Eur. J. Inorg. Chem.* **2017**, *2017*, 2435−2443.
(51) Moreau, M.; Poty, S.; Vrigneaud, J. M.; Walker, P.; Guillemin, M.; Raguin, O.; Oudot, A.; Bernhard, C.; Goze, C.; Boschetti, F.; Collin, B.; Brunotte, F.; Denat, F. MANOTA: a promising bifunctional chelating agent for copper-64 immunoPET. *Dalton Trans.* **2017**, *46*, 14659−14668.
(52) Guillou, A.; Lima, L. M. P.; Esteban-Gómez, D.; Le Poul, N.; Bartholomä, M. D.; Platas-Iglesias, C.; Delgado, R.; Patinec, V.; Tripier, R. Methylthiazolyl Tacn Ligands for Copper Complexation and Their Bifunctional Chelating Agent Derivatives for Bioconjuga-

https://doi.org/10.1021/acs.inorgchem.2c02907
Inorg. Chem. 2023, 62, 1362−1376

tion and Copper-64 Radiolabeling: An Example with Bombesin. *Inorg. Chem.* **2019**, *58*, 2669−2685.
(53) Guillou, A.; Lima, L. M. P.; Esteban-Gómez, D.; Delgado, R.; Platas-Iglesias, C.; Patinec, V.; Tripier, R. endo- versus exo-Cyclic coordination in copper complexes with methylthiazolylcarboxylate tacn derivatives. *Dalton Trans.* **2019**, *48*, 8740−8755.
(54) Pickel, T. C.; Karahalis, G. J.; Buru, C. T.; Bacsa, J.; Scarborough, C. C. Synthesis of Previously Inaccessible Derivatives of 1,4,7-Tri −R-1,4,7-Triazacyclononane, Including Chiral Examples, and a Rapid Synthesis of the HCl Salts of H₃ tacn and H₄ dtne. *Eur. J. Org. Chem.* **2018**, *2018*, 6876−6889.
(55) Roger, M.; Lima, L. M. P.; Frindel, M.; Platas-Iglesias, C.; Gestin, J.-F.; Delgado, R.; Patinec, V.; Tripier, R. Monopicolinate-dipicolyl Derivative of Triazacyclononane for Stable Complexation of Cu^{2+} and $^{64}Cu^{2+}$. *Inorg. Chem.* **2013**, *52*, 5246−5259.
(56) Gotzmann, C.; Braun, F.; Bartholomä, M. D. Synthesis,64Cu-labeling and PET imaging of 1,4,7-triazacyclononane derived chelators with pendant azaheterocyclic arms. *RSC Adv.* **2016**, *6*, 119−131.
(57) De Almeida, V. R.; Xavier, F. R.; Osório, R. E. H. M. B.; Bessa, L. M.; Schilling, E. L.; Costa, T. G.; Bortolotto, T.; Cavalett, A.; Castro, F. A. V.; Vilhena, F.; Alves, O. C.; Terenzi, H.; Eleutherio, E. C. A.; Pereira, M. D.; Haase, W.; Tomkowicz, Z.; Szpoganicz, B.; Bortoluzzi, A. J.; Neves, A. In vitro and in vivo activity of a new unsymmetrical dinuclear copper complex containing a derivative ligand of 1,4,7-triazacyclononane: catalytic promiscuity of [Cu2(L)-Cl3]. *Dalton Trans.* **2013**, *42*, 7059.
(58) Roger, M.; Patinec, V.; Tripier, R.; Triki, S.; Poul, N. L.; Mest, Y. L. Synthesis of an unsymmetrical N-functionalized triazacyclononane ligand and its Cu(II) complex. *Inorg. Chim. Acta* **2014**, *417*, 201−207.
(59) Le Fur, M.; Beyler, M.; Le Poul, N.; Lima, L. M. P.; Le Mest, Y.; Delgado, R.; Platas-Iglesias, C.; Patinec, V.; Tripier, R. Improving the stability and inertness of Cu(<scp>ii</scp>) and Cu(<scp>i</scp>) complexes with methylthiazolyl ligands by tuning the macrocyclic structure. *Dalton Trans.* **2016**, *45*, 7406−7420.
(60) Juran, S.; Walther, M.; Stephan, H.; Bergmann, R.; Steinbach, J.; Kraus, W.; Emmerling, F.; Comba, P. Hexadentate Bispidine Derivatives as Versatile Bifunctional Chelate Agents for Copper(II) Radioisotopes. *Bioconjugate Chem.* **2009**, *20*, 347−359.
(61) Singh, G.; Zarschler, K.; Hunoldt, S.; Martínez, I. I. S.; Ruehl, C. L.; Matterna, M.; Bergmann, R.; Máthé, D.; Hegedüs, N.; Bachmann, M.; Comba, P.; Stephan, H. Versatile Bispidine-Based Bifunctional Chelators for 64 Cu II -Labelling of Biomolecules. *Chem. −Eur. J.* **2020**, *26*, 1989−2001.
(62) Comba, P.; Kubeil, M.; Pietzsch, J.; Rudolf, H.; Stephan, H.; Zarschler, K. Bispidine Dioxotetraaza Macrocycles: A New Class of Bispidines for ^{64}Cu PET Imaging. *Inorg. Chem.* **2014**, *53*, 6698−6707.
(63) Roux, A.; Gillet, R.; Huclier-Markai, S.; Ehret-Sabatier, L.; Charbonnière, L. J.; Nonat, A. M. Bifunctional bispidine derivatives for copper-64 labelling and positron emission tomography. *Org. Biomol. Chem.* **2017**, *15*, 1475−1483.
(64) Comba, P.; Kerscher, M.; Rück, K.; Starke, M. Bispidines for radiopharmaceuticals. *Dalton Trans.* **2018**, *47*, 9202−9220.
(65) Comba, P.; Lienke, A. Bispidine Copper(II) Compounds: Effects of the Rigid Ligand Backbone. *Inorg. Chem.* **2001**, *40*, 5206−5209.
(66) Comba, P.; Haaf, C.; Wadepohl, H. Novel Bispidine Ligands and Their First-Row Transition Metal Complexes: Trigonal Bipyramidal and Trigonal Prismatic Geometries. *Inorg. Chem.* **2009**, *48*, 6604−6614.
(67) Fähnemann, S.; Stephan, H.; Steinbach, J.; Haaf, C.; Comba, P. Very stable CuII complexes of bispidines and their radiopharmaceutical behavior. *Nucl. Med. Biol.* **2010**, *37*, 678−679.
(68) Comba, P.; Hunoldt, S.; Morgen, M.; Pietzsch, J.; Stephan, H.; Wadepohl, H. Optimization of Pentadentate Bispidines as Bifunctional Chelators for ^{64}Cu Positron Emission Tomography (PET). *Inorg. Chem.* **2013**, *52*, 8131−8143.
(69) Comba, P.; Grimm, L.; Orvig, C.; Rück, K.; Wadepohl, H. Synthesis and Coordination Chemistry of Hexadentate Picolinic Acid Based Bispidine Ligands. *Inorg. Chem.* **2016**, *55*, 12531−12543.
(70) Comba, P.; Starke, M.; Wadepohl, H. Optimization of Hexadentate Bispidine Ligands as Chelators for $^{64}Cu^{II}$ PET Imaging. *ChemPlusChem* **2018**, *83*, 597−604.
(71) Comba, P.; Jakob, M.; Rück, K.; Wadepohl, H. Tuning of the properties of a picolinic acid-based bispidine ligand for stable copper(II) complexation. *Inorg. Chim. Acta* **2018**, *481*, 98−105.
(72) Ma, M. T.; Karas, J. A.; White, J. M.; Scanlon, D.; Donnelly, P. S. A new bifunctional chelator for copper radiopharmaceuticals: a cage amine ligand with a carboxylate functional group for conjugation to peptides. *Chem. Commun.* **2009**, *22*, 3237.
(73) Ma, M. T.; Cooper, M. S.; Paul, R. L.; Shaw, K. P.; Karas, J. A.; Scanlon, D.; White, J. M.; Blower, P. J.; Donnelly, P. S. Macrobicyclic Cage Amine Ligands for Copper Radiopharmaceuticals: A Single Bivalent Cage Amine Containing Two Lys^3-bombesin Targeting Peptides. *Inorg. Chem.* **2011**, *50*, 6701−6710.
(74) Paterson, B. M.; Roselt, P.; Denoyer, D.; Cullinane, C.; Binns, D.; Noonan, W.; Jeffery, C. M.; Price, R. I.; White, J. M.; Hicks, R. J.; Donnelly, P. S. PET imaging of tumours with a ^{64}Cu labeled macrobicyclic cage amine ligand tethered to Tyr^3-octreotate. *Dalton Trans.* **2014**, *43*, 1386−1396.
(75) Alt, K.; Paterson, B. M.; Ardipradja, K.; Schieber, C.; Buncic, G.; Lim, B.; Poniger, S. S.; Jakoby, B.; Wang, X.; O'Keefe, G. J.; Tochon-Danguy, H. J.; Scott, A. M.; Ackermann, U.; Peter, K.; Donnelly, P. S.; Hagemeyer, C. E. Single-Chain Antibody Conjugated to a Cage Amine Chelator and Labeled with Positron-Emitting Copper-64 for Diagnostic Imaging of Activated Platelets. *Mol. Pharmaceutics* **2014**, *11*, 2855−2863.
(76) Gourni, E.; Del Pozzo, L.; Kheirallah, E.; Smerling, C.; Waser, B.; Reubi, J.-C.; Paterson, B. M.; Donnelly, P. S.; Meyer, P. T.; Maecke, H. R. Copper-64 Labeled Macrobicyclic Sarcophagine Coupled to a GRP Receptor Antagonist Shows Great Promise for PET Imaging of Prostate Cancer. *Mol. Pharmaceutics* **2015**, *12*, 2781−2790.
(77) Paterson, B. M.; Buncic, G.; McInnes, L. E.; Roselt, P.; Cullinane, C.; Binns, D. S.; Jeffery, C. M.; Price, R. I.; Hicks, R. J.; Donnelly, P. S. Bifunctional ^{64}Cu-labelled macrobicyclic cage amine isothiocyanates for immuno-positron emission tomography. *Dalton Trans.* **2015**, *44*, 4901−4909.
(78) Hicks, R. J.; Jackson, P.; Kong, G.; Ware, R. E.; Hofman, M. S.; Pattison, D. A.; Akhurst, T. A.; Drummond, E.; Roselt, P.; Callahan, J.; Price, R.; Jeffery, C. M.; Hong, E.; Noonan, W.; Herschtal, A.; Hicks, L. J.; Hedt, A.; Harris, M.; Paterson, B. M.; Donnelly, P. S. ^{64}Cu-SARTATE PET Imaging of Patients with Neuroendocrine Tumors Demonstrates High Tumor Uptake and Retention, Potentially Allowing Prospective Dosimetry for Peptide Receptor Radionuclide Therapy. *J. Nucl. Med.* **2019**, *60*, 777−785.
(79) Cullinane, C.; Jeffery, C. M.; Roselt, P. D.; Van Dam, E. M.; Jackson, S.; Kuan, K.; Jackson, P.; Binns, D.; Van Zuylekom, J.; Harris, M. J.; Hicks, R. J.; Donnelly, P. S. Peptide Receptor Radionuclide Therapy with ^{67}Cu-CuSarTATE Is Highly Efficacious Against a Somatostatin-Positive Neuroendocrine Tumor Model. *J. Nucl. Med.* **2020**, *61*, 1800−1805.
(80) Bernhardt, P. V.; Harrowfield, J. M.; Hockless, D. C. R.; Sargeson, A. M. N-Methylated Macrobicyclic Hexaamines of Copper(II) and Nickel(II): Large Steric Effects. *Inorg. Chem.* **1994**, *33*, 5659−5670.
(81) Bernhardt, P. V.; Bramley, R.; Engelhardt, L. M.; Harrowfield, J. M.; Hockless, D. C. R.; Korybut-Daszkiewicz, B. R.; Krausz, E. R.; Morgan, T.; Sargeson, A. M. Copper(II) Complexes of Substituted Macrobicyclic Hexaamines: Combined Trigonal and Tetragonal Distortions. *Inorg. Chem.* **1995**, *34*, 3589−3599.
(82) Voss, S. D.; Smith, S. V.; Dibartolo, N.; McIntosh, L. J.; Cyr, E. M.; Bonab, A. A.; Dearling, J. L. J.; Carter, E. A.; Fischman, A. J.; Treves, S. T.; Gillies, S. D.; Sargeson, A. M.; Huston, J. S.; Packard, A. B. Positron emission tomography (PET) imaging of neuroblastoma

https://doi.org/10.1021/acs.inorgchem.2c02907
Inorg. Chem. 2023, 62, 1362−1376

and melanoma with ^{64}Cu-SarAr immunoconjugates. *Proc. Natl. Acad. Sci. U. S. A.* **2007**, *104*, 17489−17493.
(83) Qin, C.-J.; James, L.; Chartres, J. D.; Alcock, L. J.; Davis, K. J.; Willis, A. C.; Sargeson, A. M.; Bernhardt, P. V.; Ralph, S. F. An Unusually Flexible Expanded Hexaamine Cage and Its Cu^{II} Complexes: Variable Coordination Modes and Incomplete Encapsulation. *Inorg. Chem.* **2011**, *50*, 9131−9140.
(84) Engelhardt, L. M.; Grøndahl, L.; Harrowfield, J. M.; Ralph, S. F.; Sargeson, A. M.; Skelton, B. W.; Sobolev, A. N.; White, A. H. Copper(II) environments in some macrobicycle complexes at room and low temperatures: some novel binuclear chloro-bridged systems. *J. Inclusion Phenom. Macrocyclic Chem.* **2011**, *71*, 353−362.
(85) Mume, E.; Asad, A.; Di Bartolo, N. M.; Kong, L.; Smith, C.; Sargeson, A. M.; Price, R.; Smith, S. V. Synthesis of hexa aza cages, SarAr-NCS and AmBaSar and a study of their metal complexation, conjugation to nanomaterials and proteins for application in radioimaging and therapy. *Dalton Trans.* **2013**, *42*, 14402.
(86) Donnelly, P. S.; Harrowfield, J. M.; Skelton, B. W.; White, A. H. Carboxymethylated Cage Amines: Coordination and Lactamization. *Inorg. Chem.* **2001**, *40*, 5645−5652.
(87) Di Bartolo, N.; Sargeson, A. M.; Smith, S. V. New 64Cu PET imaging agents for personalised medicine and drug development using the hexa-aza cage, SarAr. *Org. Biomol. Chem.* **2006**, *4*, 3350.
(88) Di Bartolo, N. M.; Sargeson, A. M.; Donlevy, T. M.; Smith, S. V. Synthesis of a new cage ligand, SarAr, and its complexation with selected transition metal ions for potential use in radioimaging†. *J. Chem. Soc., Dalton Trans.* **2001**, *15*, 2303−2309.
(89) Donnelly, P. S.; Harrowfield, J. M.; Skelton, B. W.; White, A. H. Carboxymethylation of Cage Amines: Control of Alkylation by Metal Ion Coordination. *Inorg. Chem.* **2000**, *39*, 5817−5830.
(90) Kumar, K.; Tweedle, M. F.; Malley, M. F.; Gougoutas, J. Z. Synthesis, Stability, and Crystal Structure Studies of Some Ca2+, Cu2+, and Zn2+ Complexes of Macrocyclic Polyamino Carboxylates. *Inorg. Chem.* **1995**, *34*, 6472−6480.
(91) Geraldes, C. F. G. C.; Marques, M. P. M.; Castro, B. D.; Pereira, E. Study of Copper(II) Polyazamacrocyclic Complexes by Electronic Absorption Spectrophotometry and EPR Spectroscopy. *Eur. J. Inorg. Chem.* **2000**, *2000*, 559−565.
(92) Takács, A.; Napolitano, R.; Purgel, M.; Bényei, A. C.; Zékány, L.; Brücher, E.; Tóth, I.; Baranyai, Z.; Aime, S. Solution Structures, Stabilities, Kinetics, and Dynamics of DO3A and DO3A−Sulphonamide Complexes. *Inorg. Chem.* **2014**, *53*, 2858−2872.
(93) Prenesti, E.; Daniele, P. G.; Berto, S.; Toso, S. Spectrum−structure correlation for visible absorption spectra of copper(II) complexes showing axial co-ordination in aqueous solution. *Polyhedron* **2006**, *25*, 2815−2823.
(94) Toth, E.; Brucher, E.; Lazar, I.; Toth, I. Kinetics of Formation and Dissociation of Lanthanide(III)-DOTA Complexes. *Inorg. Chem.* **1994**, *33*, 4070−4076.
(95) Burai, L.; Fábián, I.; Király, R.; Szilágyi, E.; Brücher, E. Equilibrium and kinetic studies on the formation of the lanthanide(III) complexes, [Ce(dota)]− and [Yb(dota)]− (H4dota = 1,4,7,10-tetraazacyclododecane-1,4,7,10-tetraacetic acid). *J. Chem. Soc., Dalton Trans.* **1998**, *2*, 243−248.
(96) Szilágyi, E.; Tóth, É.; Kovács, Z.; Platzek, J.; Radüchel, B.; Brücher, E. Equilibria and formation kinetics of some cyclen derivative complexes of lanthanides. *Inorg. Chim. Acta* **2000**, *298*, 226−234.
(97) Chang, C. A.; Francesconi, L. C.; Malley, M. F.; Kumar, K.; Gougoutas, J. Z.; Tweedle, M. F.; Lee, D. W.; Wilson, L. J. Synthesis, characterization, and crystal structures of M(DO3A) (M = iron, gadolinium) and Na[M(DOTA)] (M = Fe, yttrium, Gd). *Inorg. Chem.* **1993**, *32*, 3501−3508.
(98) Balogh, E.; Tripier, R.; Fousková, P.; Reviriego, F.; Handel, H.; Tóth, É. Monopropionate analogues of DOTA4− and DTPA5−: kinetics of formation and dissociation of their lanthanide(iii) complexes. *Dalton Trans.* **2007**, *32*, 3572.
(99) Wang, X.; Jin, T.; Comblin, V.; Lopez-Mut, A.; Merciny, E.; Desreux, J. F. A kinetic investigation of the lanthanide DOTA chelates. Stability and rates of formation and of dissociation of a macrocyclic gadolinium(III) polyaza polycarboxylic MRI contrast agent. *Inorg. Chem.* **1992**, *31*, 1095−1099.
(100) Tircso, G.; Webber, B. C.; Kucera, B. E.; Young, V. G.; Woods, M. Analysis of the Conformational Behavior and Stability of the SAP and TSAP Isomers of Lanthanide(III) NB-DOTA-Type Chelates. *Inorg. Chem.* **2011**, *50*, 7966−7979.
(101) Pérez-Malo, M.; Szabó, G.; Eppard, E.; Vagner, A.; Brücher, E.; Tóth, I.; Maiocchi, A.; Suh, E. H.; Kovács, Z.; Baranyai, Z.; Rösch, F. Improved Efficacy of Synthesizing $*M^{III}$-Labeled DOTA Complexes in Binary Mixtures of Water and Organic Solvents. A Combined Radio- and Physicochemical Study. *Inorg. Chem.* **2018**, *57*, 6107−6117.
(102) Stenson, P. A.; Thompson, A. L.; Parker, D. Structural characterisation of a diprotonated ligand lanthanide complex—a key intermediate in lanthanide ion association and complex dissociation pathways. *Dalton Trans.* **2006**, *27*, 3291−3293.
(103) Lin, C.-C.; Chen, C.-L.; Liu, K.-Y.; Chang, C. A. Dissociation kinetics of macrocyclic trivalent lanthanide complexes of 1,4,7,10-tetraazacyclododecane-1,7-diacetic acid (DO2A). *Dalton Trans.* **2011**, *40*, 6268.
(104) Jackson, J. A.; Linero, V.; Bessen, N. P.; Nash, K. L.; Shafer, J. C. Leveraging slow DOTA f-element complexation kinetics to enable separations by kinetic design. *Sep. Purif. Technol.* **2021**, *274*, No. 118919.
(105) Audras, M.; Berthon, L.; Berthon, C.; Guillaumont, D.; Dumas, T.; Illy, M.-C.; Martin, N.; Zilbermann, I.; Moiseev, Y.; Ben-Eliyahu, Y.; Bettelheim, A.; Cammelli, S.; Hennig, C.; Moisy, P. Structural Characterization of Am(III)- and Pu(III)-DOTA Complexes. *Inorg. Chem.* **2017**, *56*, 12248−12259.
(106) Balogh, E.; Tripier, R.; Ruloff, R.; Tóth, É. Kinetics of formation and dissociation of lanthanide(<scp>iii</scp>) complexes with the 13-membered macrocyclic ligand $TRITA^{4-}$. *Dalton Trans.* **2005**, *6*, 1058−1065.
(107) Balogh, E.; Tripier, R.; Ruloff, R.; Tóth, É. Kinetics of formation and dissociation of lanthanide(iii) complexes with the 13-membered macrocyclic ligand TRITA4−. *Dalton Trans.* **2005**, *6*, 1058−1065.
(108) Meyer, M.; Dahaoui-Gindrey, V.; Lecomte, C.; Guilard, R. Conformations and coordination schemes of carboxylate and carbamoyl derivatives of the tetraazamacrocycles cyclen and cyclam, and the relation to their protonation states. *Coord. Chem. Rev.* **1998**, *178*−*180*, 1313−1405.
(109) Kumar, K.; Chang, C. A.; Francesconi, L. C.; Dischino, D. D.; Malley, M. F.; Gougoutas, J. Z.; Tweedle, M. F. Synthesis, Stability, and Structure of Gadolinium(III) and Yttrium(III) Macrocyclic Poly(amino carboxylates). *Inorg. Chem.* **1994**, *33*, 3567−3575.
(110) Barbaro, P.; Bianchini, C.; Capannesi, G.; Di Luca, L.; Laschi, F.; Petroni, D.; Salvadori, P. A.; Vacca, A.; Vizza, F. Synthesis and characterization of the tetraazamacrocycle 4,10-dimethyl-1,4,7,10-tetraazacyclododecane-1,7-diacetic acid (H2Me2DO2A) and of its neutral copper(II) complex [Cu(Me2DO2A)]. A new 64Cu-labeled macrocyclic complex for positron emission tomography imaging. *J. Chem. Soc., Dalton Trans.* **2000**, *14*, 2393−2401.
(111) Silversides, J. D.; Allan, C. C.; Archibald, S. J. Copper(ii) cyclam-based complexes for radiopharmaceutical applications: synthesis and structural analysis. *Dalton Trans.* **2007**, *9*, 971−978.
(112) Halcrow, M. A. Jahn−Teller distortions in transition metal compounds, and their importance in functional molecular and inorganic materials. *Chem. Soc. Rev.* **2013**, *42*, 1784−1795.
(113) Murphy, B.; Hathaway, B. The stereochemistry of the copper(II) ion in the solid-state—some recent perspectives linking the Jahn−Teller effect, vibronic coupling, structure correlation analysis, structural pathways and comparative X-ray crystallography. *Coord. Chem. Rev.* **2003**, *243*, 237−262.
(114) Wieghardt, K.; Bossek, U.; Chaudhuri, P.; Herrmann, W.; Menke, B. C.; Weiss, J. 1,4,7-Triazacyclononane-N,N′,N″-triacetate (TCTA), a new hexadentate ligand for divalent and trivalent metal ions. Crystal structures of [CrIII(TCTA)], [FeIII(TCTA)], and

https://doi.org/10.1021/acs.inorgchem.2c02907
Inorg. Chem. 2023, 62, 1362−1376

Na[CuII(TCTA)].bul.2NaBr.bul.8H2O. *Inorg. Chem.* **1982**, *21*, 4308−4314.
(115) Li, Q.-X.; Li, Q.; Chen, R.; Yang, X.-L.; Zhou, J.-Y.; Xu, H.-B. Synthesis, structure and superoxide dismutase activity of a novel tetranuclear copper(II) complex Na2[Cu4Na2(TACNTA)4(H2O)-6]·(H2O)26. *Inorg. Chem. Commun.* **2010**, *13*, 1293−1295.
(116) Wei, Q.; Tang, Q.; Feng, Y.-F.; Zhang, Z.; Liao, Y.-Z. Preparation, crystal structures and magnetic properties of hetero- and homo-metallic coordination polymers with triazacyclononane derivatives bearing propionic acid pendant arms. *Transition Met. Chem.* **2017**, *42*, 41−50.
(117) Phetmung, H.; Runpet, T.; Choosiri, N. Roles of a unique apical salicylate ligand of neutral [Cu(phen) (Hsal)2(H2O)] to coordination mode, geometry, weak interactions, thermal analysis and spectroscopy. *J. Mol. Struct.* **2019**, *1178*, 500−507.
(118) Du, M.; Bu, X.-H. Synthesis, spectra and crystal structure of a CuII complex exhibiting novel two-dimensional joint-ladder like hydrogen-bonding pattern with an amino-acid type diazamesocyclic ligand. *J. Mol. Struct.* **2004**, *692*, 195−199.
(119) Garribba, E.; Micera, G. The Determination of the Geometry of Cu(II) Complexes: An EPR Spectroscopy Experiment. *J. Chem. Educ.* **2006**, *83*, 1229.
(120) Rojas-González, P. X.; Choquesillo-Lazarte, D.; González-Pérez, J. M.; Ruíz- García, S. A.; Carballo, R.; Castiñeiras, A.; Niclós-Gutiérrez, J. Synthesis, crystal structure and properties of N-tert-butyliminodiacetic acid (H2TEBIDA), [Cu(TEBIDA)(H2O)2], {[Cu(TEBIDA)(Him)]·2H2O}n, {Cu(TEBIDA) (5MeHim)·H2O}n, and [Cu(TEBIDA)(2,2′-bipy)(H2O)]·4.5H2O, (Him=imidazole, 5MeImH=5-methylimidazole and 2,2′-bipy=2,2′-bipyridine). *Polyhedron* **2003**, *22*, 1027−1037.
(121) Łabanowska, M.; Bidzińska, E.; Para, A.; Kurdziel, M. EPR investigation of Cu(II)-complexes with nitrogen derivatives of dialdehyde starch. *Carbohydr. Polym.* **2012**, *87*, 2605−2613.
(122) Kivelson, D.; Neiman, R. ESR Studies on the Bonding in Copper Complexes. *J. Chem. Phys.* **1961**, *35*, 149−155.
(123) Yokoi, H.; Addison, A. W. Spectroscopic and redox properties of pseudotetrahedral copper(II) complexes. Their relation to copper proteins. *Inorg. Chem.* **1977**, *16*, 1341−1349.
(124) McGarvey, B. R. The isotropic hyperfine interaction. *J. Phys. Chem. A* **1967**, *71*, 51−66.
(125) Peisach, J.; Blumberg, W. E. Structural implications derived from the analysis of electron paramagnetic resonance spectra of natural and artificial copper proteins. *Arch. Biochem. Biophys.* **1974**, *165*, 691−708.
(126) Zhao, Y.; Truhlar, D. G. A new local density functional for main-group thermochemistry, transition metal bonding, thermochemical kinetics, and noncovalent interactions. *J. Chem. Phys.* **2006**, *125*, 194101.
(127) Delgado, R.; da Silva, J. J. R. F. Metal complexes of cyclic tetra-azatetra-acetic acids. *Talanta* **1982**, *29*, 815−822.
(128) Determan, J. J.; Poole, K.; Scalmani, G.; Frisch, M. J.; Janesko, B. G.; Wilson, A. K. Comparative Study of Nonhybrid Density Functional Approximations for the Prediction of 3d Transition Metal Thermochemistry. *J. Chem. Theory Comput.* **2017**, *13*, 4907−4913.
(129) Moltved, K. A.; Kepp, K. P. Chemical Bond Energies of 3d Transition Metals Studied by Density Functional Theory. *J. Chem. Theory Comput.* **2018**, *14*, 3479−3492.
(130) Iron, M. A.; Janes, T. Evaluating Transition Metal Barrier Heights with the Latest Density Functional Theory Exchange−Correlation Functionals: The MOBH35 Benchmark Database. *J. Phys. Chem. A* **2019**, *123*, 3761−3781.
(131) Abu-Nawwas, A.-A. H.; Mason, P. V.; Milway, V. A.; Muryn, C. A.; Pritchard, R. J.; Tuna, F.; Collison, D.; Winpenny, R. E. P. Synthesis of new polymetallic iron(iii) clusters containing polycarboxylate ligands based on cavity-blocked cyclen. *Dalton Trans.* **2008**, *2*, 198−200.
(132) Heroux, K. J.; Woodin, K. S.; Tranchemontagne, D. J.; Widger, P. C. B.; Southwick, E.; Wong, E. H.; Weisman, G. R.; Tomellini, S. A.; Wadas, T. J.; Anderson, C. J.; Kassel, S.; Golen, J. A.; Rheingold, A. L. The long and short of it: the influence of N-carboxyethyl versus N-carboxymethyl pendant arms on in vitro and in vivo behavior of copper complexes of cross-bridged tetraamine macrocycles. *Dalton Trans.* **2007**, *21*, 2150−2162.
(133) Kálmán, F. K.; Baranyai, Z.; Tóth, I.; Bányai, I.; Király, R.; Brücher, E.; Aime, S.; Sun, X.; Sherry, A. D.; Kovács, Z. Synthesis, Potentiometric, Kinetic, and NMR Studies of 1,4,7,10-Tetraazacyclododecane-1,7-bis(acetic acid)-4,10-bis(methylenephosphonic acid) (DO2A2P) and its Complexes with Ca(II), Cu(II), Zn(II) and Lanthanide(III) Ions. *Inorg. Chem.* **2008**, *47*, 3851−3862.
(134) Prasanphanich Adam, F.; Nanda Prasant, K.; Rold Tammy, L.; Ma, L.; Lewis Michael, R.; Garrison Jered, C.; Hoffman Timothy, J.; Sieckman Gary, L.; Figueroa Said, D.; Smith Charles, J. [64Cu-NOTA-8-Aoc-BBN(7-14)NH2] targeting vector for positron-emission tomography imaging of gastrin-releasing peptide receptor-expressing tissues. *Proc. Natl. Acad. Sci. U. S. A.* **2007**, *104*, 12462−12467.
(135) White, J. B.; Hu, L. Y.; Boucher, D. L.; Sutcliffe, J. L. ImmunoPET Imaging of *αvβ6* Expression Using an Engineered Anti-*αvβ6* Cys-diabody Site-Specifically Radiolabeled with Cu-64: Considerations for Optimal Imaging with Antibody Fragments. *Mol. Imaging Biol.* **2018**, *20*, 103−113.
(136) Bevilacqua, A.; Gelb, R. I.; Hebard, W. B.; Zompa, L. J. Equilibrium and thermodynamic study of the aqueous complexation of 1,4,7-triazacyclononane-N,N′,N″-triacetic acid with protons, alkaline-earth-metal cations, and copper(II). *Inorg. Chem.* **1987**, *26*, 2699−2706.
(137) Wadas, T. J.; Wong, E. H.; Weisman, G. R.; Anderson, C. J. Coordinating Radiometals of Copper, Gallium, Indium, Yttrium, and Zirconium for PET and SPECT Imaging of Disease. *Chem. Rev.* **2010**, *110*, 2858−2902.
(138) Pandya, D. N.; Kim, J. Y.; Park, J. C.; Lee, H.; Phapale, P. B.; Kwak, W.; Choi, T. H.; Cheon, G. J.; Yoon, Y.-R.; Yoo, J. Revival of TE2A; a better chelate for Cu(II) ions than TETA? *Chem. Commun.* **2010**, *46*, 3517−3519.
(139) Dale, A. V.; An, G. I.; Pandya, D. N.; Ha, Y. S.; Bhatt, N.; Soni, N.; Lee, H.; Ahn, H.; Sarkar, S.; Lee, W.; Huynh, P. T.; Kim, J. Y.; Gwon, M.-R.; Kim, S. H.; Park, J. G.; Yoon, Y.-R.; Yoo, J. Synthesis and Evaluation of New Generation Cross-Bridged Bifunctional Chelator for 64Cu Radiotracers. *Inorg. Chem.* **2015**, *54*, 8177−8186.
(140) Pandya, D. N.; Dale, A. V.; Kim, J. Y.; Lee, H.; Ha, Y. S.; An, G. I.; Yoo, J. New Macrobicyclic Chelator for the Development of Ultrastable64Cu-Radiolabeled Bioconjugate. *Bioconjugate Chem.* **2012**, *23*, 330−335.
(141) Anderson, J. L.; Shain, I. Cyclic voltammetric studies of the pH dependence of copper(II) reduction in acidic aqueous nitrate and perchlorate solutions. *Anal. Chem.* **1976**, *48*, 1274−1282.
(142) García-Rodríguez, D. E.; Mendoza-Huizar, L. H.; Rios-Reyes, C. H.; Alatorre-Ordaz, M. A. Copper electrodeposition on glassy carbon and highly oriented pyrolytic graphite substrates from perchlorate solutions. *Química Nova* **2012**, *35*, 699−704.
(143) Randles, J. E. B. 142. The equilibrium between cuprous and cupric compounds in presence of metallic copper. *J. Chem. Soc.* **1941**, 802.
(144) Ukpong, E.; Udoetok, I.; Akpanudo, N. Cyclic Voltammetry of Aqueous Copper (II)- Pentamethyldiethylenetriamine Systems at Various pH Values. *Russ. J. Appl. Chem.* **2013**, *5*, 50.
(145) Weberg, A. B.; Murphy, R. P.; Tomson, N. C. Oriented internal electrostatic fields: an emerging design element in coordination chemistry and catalysis. *Chem. Sci.* **2022**, *13*, 5432−5446.
(146) Wang, J.; Yang, C.-T.; Kim, Y.-S.; Sreerama, S. G.; Cao, Q.; Li, Z.-B.; He, Z.; Chen, X.; Liu, S. 64Cu-Labeled Triphenylphosphonium and Triphenylarsonium Cations as Highly Tumor-Selective Imaging Agents. *J. Med. Chem.* **2007**, *50*, 5057−5069.
(147) Idris, N. S.; Barlow, J. M.; Chabolla, S. A.; Ziller, J. W.; Yang, J. Y. Synthesis and redox properties of heterobimetallic Re(bpyCrown-M)(CO)3Cl complexes, where M = Na+, K+, Ca2+, and Ba2+. *Polyhedron* **2021**, *208*, No. 115385.

https://doi.org/10.1021/acs.inorgchem.2c02907
Inorg. Chem. 2023, 62, 1362−1376

(148) Barlow, J. M.; Ziller, J. W.; Yang, J. Y. Inhibiting the Hydrogen Evolution Reaction (HER) with Proximal Cations: A Strategy for Promoting Selective Electrocatalytic Reduction. *ACS Catal.* **2021**, *11*, 8155−8164.
(149) Robinson, J. R.; Gordon, Z.; Booth, C. H.; Carroll, P. J.; Walsh, P. J.; Schelter, E. J. Tuning Reactivity and Electronic Properties through Ligand Reorganization within a Cerium Heterobimetallic Framework. *J. Am. Chem. Soc.* **2013**, *135*, 19016−19024.
(150) Ambundo, E. A.; Deydier, M.-V.; Grall, A. J.; Aguera-Vega, N.; Dressel, L. T.; Cooper, T. H.; Heeg, M. J.; Ochrymowycz, L. A.; Rorabacher, D. B. Influence of Coordination Geometry upon Copper(II/I) Redox Potentials. Physical Parameters for Twelve Copper Tripodal Ligand Complexes. *Inorg. Chem.* **1999**, *38*, 4233−4242.
(151) Vivier, D.; Sharma, S. K.; Zeglis, B. M. Understanding the in vivo fate of radioimmunoconjugates for nuclear imaging. *J. Labelled Compd. Radiopharm.* **2018**, *61*, 672−692.
(152) Xiao, Z.; Donnelly, P. S.; Zimmermann, M.; Wedd, A. G. Transfer of Copper between Bis(thiosemicarbazone) Ligands and Intracellular Copper-Binding Proteins. Insights into Mechanisms of Copper Uptake and Hypoxia Selectivity. *Inorg. Chem.* **2008**, *47*, 4338−4347.
(153) Poschenrieder, A.; Schottelius, M.; Osl, T.; Schwaiger, M.; Wester, H.-J. [64Cu]NOTA-pentixather enables high resolution PET imaging of CXCR4 expression in a preclinical lymphoma model. *EJNMMI Radiopharm. Chem.* **2017**, *2*, 2.
(154) Cooper, M. S.; Ma, M. T.; Sunassee, K.; Shaw, K. P.; Williams, J. D.; Paul, R. L.; Donnelly, P. S.; Blower, P. J. Comparison of 64Cu-Complexing Bifunctional Chelators for Radioimmunoconjugation: Labeling Efficiency, Specific Activity, and in Vitro/in Vivo Stability. *Bioconjugate Chem.* **2012**, *23*, 1029−1039.
(155) Le Fur, M.; Beyler, M.; Le Poul, N.; Lima, L. M. P.; Le Mest, Y.; Delgado, R.; Platas-Iglesias, C.; Patinec, V.; Tripier, R. Improving the stability and inertness of Cu(ii) and Cu(i) complexes with methylthiazolyl ligands by tuning the macrocyclic structure. *Dalton Trans.* **2016**, *45*, 7406−7420.
(156) Ogino, H. The Stability Constants of Ethylenediaminetetraacetato, Trimethylenediaminetetraacetato and Propylenediaminetetraacetato Complexes of Some Divalent Metal Ions. *Bull. Chem. Soc. Jpn.* **1965**, *38*, 771−777.
(157) Anderegg, G.Critical Survey Of Stability Constants of Edta Complexes. In *Critical Survey of Stability Constants of EDTA Complexes*, Anderegg, G., Ed.; Pergamon, 1977; pp 1−36.
(158) Jagadish, B.; Brickert-Albrecht, G. L.; Nichol, G. S.; Mash, E. A.; Raghunand, N. On the synthesis of 1,4,7-tris(tert-butoxycarbonylmethyl)-1,4,7,10-tetraazacyclododecane. *Tetrahedron Lett.* **2011**, *52*, 2058−2061.
(159) Faulkner, S.; Carrié, M.-C.; Pope, S. J. A.; Squire, J.; Beeby, A.; Sammes, P. G. Pyrene-sensitised near-IR luminescence from ytterbium and neodymium complexes. *Dalton Trans.* **2004**, *9*, 1405−1409.
(160) Gans, P.; Sabatini, A.; Vacca, A. Investigation of equilibria in solution. Determination of equilibrium constants with the HYPERQUAD suite of programs. *Talanta* **1996**, *43*, 1739−1753.
(161) Gans, P.; Sabatini, A.; Vacca, A. Determination of equilibrium constants from spectrophometric data obtained from solutions of known pH : The program pHab. *Ann. Chim.* **1999**, *89*, 45−49.
(162) Cannes, C.; Kanoufi, F.; Bard, A. J. Cyclic voltammetry and scanning electrochemical microscopy of ferrocenemethanol at monolayer and bilayer-modified gold electrodes. *J. Electroanal. Chem.* **2003**, *547*, 83−91.
(163) Bourdillon, C.; Demaille, C.; Moiroux, J.; Saveant, J.-M. Catalysis and Mass Transport in Spatially Ordered Enzyme Assemblies on Electrodes. *J. Am. Chem. Soc.* **1995**, *117*, 11499−11506.
(164) Dolg, M.; Wedig, U.; Stoll, H.; Preuss, H. Energy-adjusted ab initio pseudopotentials for the first row transition elements. *J. Chem. Phys.* **1987**, *86*, 866−872.
(165) Petersson, G. A.; Bennett, A.; Tensfeldt, T. G.; Al-Laham, M. A.; Shirley, W. A.; Mantzaris, J. A complete basis set model chemistry. I. The total energies of closed-shell atoms and hydrides of the first-row elements. *J. Chem. Phys.* **1988**, *89*, 2193−2218.
(166) Peterson, G. A.; Bennett, A.; Tensfeldt, T. G.; Laham, M.; Shirley, W. A.; Manzaris, J. A complete basis set model chemistry. II. Open-shell systems and the total energies of the first-row atoms. *J. Chem. Phys.* **1991**, *94*, 6081.
(167) Marenich, A. V.; Cramer, C. J.; Truhlar, D. G. Universal Solvation Model Based on Solute Electron Density and on a Continuum Model of the Solvent Defined by the Bulk Dielectric Constant and Atomic Surface Tensions. *J. Phys. Chem. B* **2009**, *113*, 6378−6396.

https://doi.org/10.1021/acs.inorgchem.2c02907
Inorg. Chem. 2023, 62, 1362−1376